Geomorphology 388 (2021) 107787

Contents lists available at ScienceDirect

Geomorphology

journal homepage: www.elsevier.com/locate/geomorph

Reversible glacial-periglacial transition in response to climate changes and paraglacial dynamics: A case study from Héðinsdalsjökull (northern Iceland)

David Palacios [a,*], Manuel Rodríguez-Mena [a], José M. Fernández-Fernández [b], Irene Schimmelpfennig [c], Luis M. Tanarro [a], José J. Zamorano [d], Nuria Andrés [a], Jose Úbeda [a], Þorsteinn Sæmundsson [e], Skafti Brynjólfsson [f], Marc Oliva [g], A.S.T.E.R. Team [c,1]

[a] High Mountain Physical Geography Research Group, Department of Geography, Universidad Complutense de Madrid, Madrid, 28040, Madrid, Spain
[b] Instituto de Geografia e Ordenamento do Território (IGOT), Universidade de Lisboa, Lisbon, Portugal
[c] Aix-Marseille Université, CNRS, IRD, INRAE, Coll, France, UM 34 CEREGE, Technopôle de l'Environnement Arbois-Méditerranée, BP 80, 13545 Aix-en-Provence, France
[d] Institute of Geography, Universidad Nacional Autónoma de México, México DF, Mexico
[e] Faculty of Life and Environmental Science, University of Iceland, Reykjavík, Iceland
[f] Icelandic Institute of Natural History, Akureyri, Iceland
[g] Department of Geography, Universitat de Barcelona, Barcelona, Spain

ARTICLE INFO

Article history:
Received 20 February 2021
Received in revised form 17 May 2021
Accepted 17 May 2021
Available online 21 May 2021

Keywords:
Northern Iceland
Debris-covered glacier
Rock glacier
Debris-free glacier
Glacial evolution
Paraglacial dynamics
Climatic variability

ABSTRACT

The objective of this work is to chronologically establish the origin of the different glacial and rock glacier complex landforms deposited by Héðinsdalsjökull glacier (65°39′ N, 18°55′ W), in the Héðinsdalur valley (Skagafjörður fjord, Tröllaskagi peninsula, central northern Iceland). Multiple methods were applied: geomorphological analysis and mapping, glacier reconstruction and equilibrium-line altitude calculation, Cosmic-Ray Exposure dating (in situ cosmogenic ^{36}Cl), and lichenometric dating. The results reveal that a debris-free glacier receded around 6.6 ± 0.6 ka, during the Holocene Thermal Maximum. The retreat of the glacier exposed its headwall and accelerated paraglacial dynamics. As a result, the glacier terminus evolved into a debris-covered glacier and a rock glacier at a slightly higher elevation. The front of this rock glacier stabilized shortly after it formed, although nuclide inheritance is possible, but its sector close the valley head stabilized between 1.5 and 0.6 ka. The lowest part of the debris-covered glacier (between 600 and 820 m altitude) collapsed at ca. 2.4 ka. Since then, periods of glacial advance and retreat have alternated, particularly during the Little Ice Age. The maximum advance during this phase occurred in the 15th to 17th centuries with subsequent re-advances, namely at the beginning of the 19th and 20th centuries. After a significant retreat during the first decades of the 20th century, the glacier advanced in the 1960s to 1990s, and then retreated again, in accordance with the local climatic evolution. The internal ice of both the debris-covered and the rock glacier have survived until the present day, although enhanced subsidence provides evidence of their gradual degradation. A new rock glacier developed from an ice-cored moraine from around 1940–1950 CE. Thus, the Holocene coupling between paraglacial and climatic shifts has resulted in a complex evolution of Héðinsdalsjökull, which is conflicting with previously proposed models: a glacier, which had first evolved into a debris-covered and rock glacier, could later be transformed into a debris-free glacier, with a higher sensitivity to climatic variability.

1. Introduction

The distribution of glacial cirques and the diversity of the related glacial and periglacial landforms found inside them derive from complex geomorphological responses to climate variability as well as by changes of the geomorphological setting associated with the transition from glaciation to deglaciation stages (Benedict, 1973; Evans and Cox, 1974, 1995; Dahl and Nesje, 1992; Barr and Spagnolo, 2015; Barth et al., 2016; Barr et al., 2017; Ipsen et al., 2018). Indeed, the occurrence of permafrost during the paraglacial phase following cirque deglaciation enhances the readjustment of cirque walls and favors the development of complex landform assemblages (Ballantyne, 2002, 2013; Knight and Harrison, 2014; Beniston et al., 2018; Jones et al., 2019; Knight et al., 2019). The ice surface lowering and its disappearance determines the decompression of the cirque walls and the increase of debris supply onto the shrinking glaciers located beneath. This process may lead to

* Corresponding author.
E-mail address: davidp@ucm.es (D. Palacios).
[1] Consortium: Georges Aumaître, Didier Bourlès, Karim Keddadouche

https://doi.org/10.1016/j.geomorph.2021.107787

the transformation of debris-free into debris-covered glaciers in a first step, and afterwards even evolve into rock glaciers (Hambrey et al., 2008; Berthling, 2011; Monnier and Kinnard, 2015, 2016; Janke et al., 2013, 2015; Anderson et al., 2018a; Rowan et al., 2015; Jones et al., 2019; Knight et al., 2019). Although this transformation is well known, the climatic and geomorphological dynamics that control the timing of each phase involved remain unclear, as they depend on various factors, including climate, topography, lithology, degree of weathering of the slopes or tectonics, among others. (Monnier et al., 2014; Monnier and Kinnard, 2015, 2016; Emmer et al., 2015; Dusik et al., 2015; Anderson et al., 2018a; Knight et al., 2019; Jones et al., 2019). Due to the abundance and variety of debris-covered glaciers and rock glaciers in the mountains of the Tröllaskagi peninsula (central northern Iceland) (Lilleøren et al., 2013), this area constitutes a natural laboratory for the study of transformation of glaciers under the response of paraglacial dynamics to climate variability (Andrés et al., 2016). The location, typology and recent evolution of many of these features is well known in a number of valleys (Tanarro et al., 2018, 2019; Fernández-Fernández et al., 2020), but scientific knowledge on their origin and millennial-scale evolution is still limited.

The records of the deglaciation and Holocene evolution of glaciers in the Tröllaskagi peninsula suggest that only their debris-free glaciers show a great sensitivity to climatic fluctuations (i.e., glacial advance/retreat after a short response time to climatic variability such as cold spells or warming; Caseldine, 1985; Häberle, 1991; Kugelmann, 1991; Fernández-Fernández et al., 2017, 2019) while debris-covered glacier and rock glacier react to climate changes very slowly and with greater time delay (Andrés et al., 2016; Tanarro et al., 2019; Campos et al., 2019). Until the last decade, the lichenometric dating suggested that debris-covered glacier and rock glaciers were formed during Little Ice Age (LIA) mainly in 19th century (Martin et al., 1994; Hamilton and Whalley, 1995a, 1995b) or at the latest during the early Neoglacial, based on the extrapolation of surface velocities of these features (Wangensteen et al., 2006; Kellerer-Pirklbauer et al., 2007). However, recent Cosmic-Ray Exposure (CRE) dates in several of these formations reveal that they are much older (Fernández-Fernández et al., 2020), probably from the early Holocene. The lower fronts of the debris-covered and rock glaciers collapsed at ~9 ka while the upper sectors still preserve at present their inner ice (Tanarro et al., 2019; Campos et al., 2019; Fernández-Fernández et al., 2020).

Debris-free, debris-covered and rock glaciers distributed in the cirques of the Tröllaskagi peninsula are concentrated in north-exposed cirques and their snouts lie above ~900–950 m a.s.l. However, the controlling factors that result in different glacier typologies in adjacent cirques remain unknown. An exceptional case in the area is Héðinsdalsjökull glacier (Fig. 1). Its detailed geomorphological mapping revealed 10 different evolutionary phases comprising active and relict sectors of a debris-covered glacier, rock glaciers and an independent debris-free glacier overlapping them (Rodríguez-Mena et al., 2021). The lowest landform of this cirque is a collapsed debris-covered frontal moraine, which has been dated with ^{36}Cl to have stabilized at 3–2 ka (Fernández-Fernández et al., 2020).

The great complexity of this landform set offers an opportunity to study the evolution that a glacier may experience, in response to glacio-geomorphological dynamics and climate variability. Thus, the aims of this work are to (i) chronologically establish the origin of the different landforms inside the cirque; and (ii) unravel the climatic and geomorphological background that determined the genesis of each glacier type. To meet such objectives, new Cosmic-Ray Exposure (CRE) dating dates will be obtained from key landforms, in addition to previously published ones (Fernández-Fernández et al., 2020) that will be updated so that all of them are comparable. Also lichenometric dating will be applied to the most recent landforms and their evolution during the last years will be reconstructed through multitemporal analysis of historical aerial photographs.

2. Geographic setting

The Tröllaskagi peninsula is located in central northern Iceland, between the Skagafjörður and Eyjafjörður fjords, to the west and east, respectively (Fig. 1). The topographical and geological setting consists of a plateau at 1200–1330 m a.s.l. resulting from the stacking of different Miocene basaltic lava flows (Tertiary Basalt Formation) in a gently-sloping arrangement alternating with sedimentary strata (Sæmundsson et al., 1980). The plateau is deeply incised by a dense network of tributary valleys, characterized by steep and unstable slopes where rockfalls, landslides, snow avalanches and debris flows are common (Jónsson, 1976; Whalley et al., 1983; Mercier et al., 2013; Cossart et al., 2014; Decaulne et al., 2016; Sæmundsson et al., 2018; Morino et al., 2019). Over 160 glacial cirques have been accounted at the headwalls of these valleys (Caseldine and Stotter, 1993; Lilleøren et al., 2013), most of which are currently occupied by debris-covered and rock glaciers. Their fronts are located at 900–950 m, where the mean annual air temperature (MAAT) ranges between −2.6 and −1.8 °C (Etzelmüller et al., 2007).

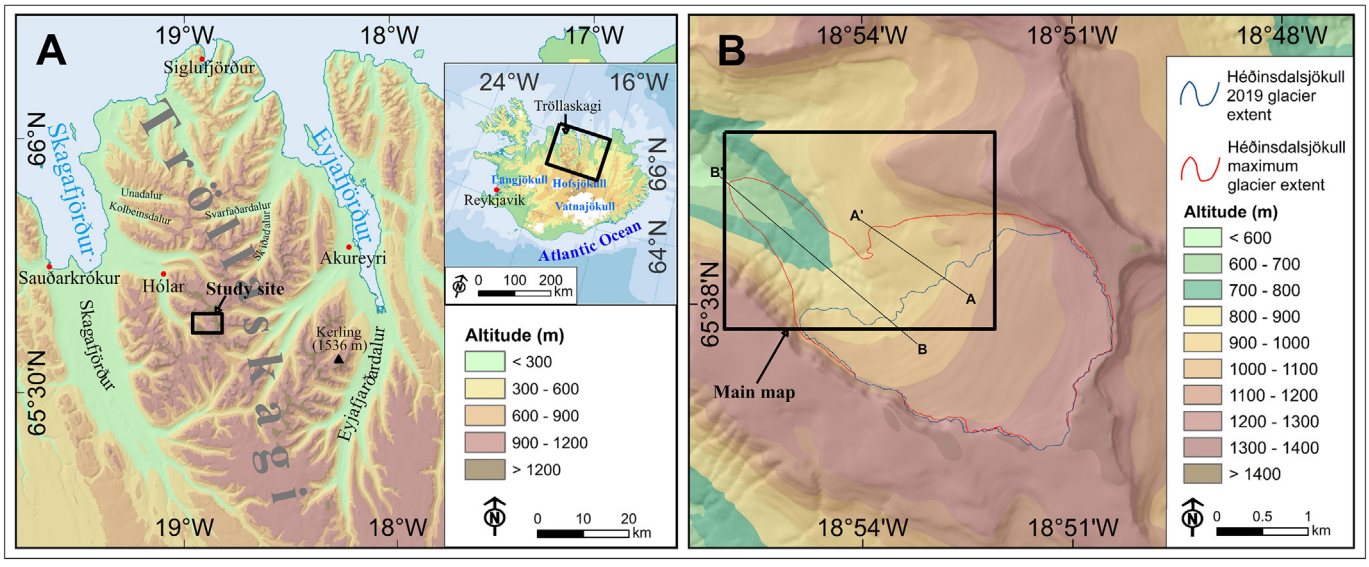

Fig. 1. Location map of the study area. A) Tröllaskagi peninsula in Northern Iceland. B) Héðinsdalur valley and maximum extent of Héðinsdalsjökull glacial landforms. The box corresponds to the area included in the geomorphological map shown in Fig. 2. The transects A-A' and B-B' of the Fig. 5 are located into the box.

The MAATs on the Tröllaskagi peninsula (1961–1990 series) range between 2 and 4 °C at the coast, and between −4 and −2 °C in the summits (Etzelmüller et al., 2007; Farbrot et al., 2007). The mean annual rainfall in the period 1971–2000 ranges from 400 mm in the coastal areas to 2500 mm in the summits (Crochet et al., 2007). The lower limit of the mountain permafrost on the Tröllaskagi peninsula remains at ~900 m according to the 1961–1990 series (Etzelmüller et al., 2007), although it ranges between 800 and 1000 m, depending on the snow cover distribution, according to 1960–2016 series (Czekirda et al., 2019). These data are confirmed by the present-day distribution of active rock glaciers (Lilleøren et al., 2013). During the Holocene Thermal Maximum (HTM), permafrost only remained in the higher areas of Tröllaskagi and spread downslope from the summits since 5–3 ka, reaching its maximum extent during the LIA (Czekirda et al., 2019; Etzelmüller et al., 2007, 2020).

Héðinsdalsjökull (65°39 ′N, 18°55′ W, between 700 and 1200 m of altitude) is located at the head of the Héðinsdalur valley. This valley is 8 km long SE-NW oriented in the upper part and turn towards E-W where it joins the Hjaltadalur valley, in the vicinity of Hólar village (Fig. 1). The whole glacier complex currently covers a total area of 7 km^2.

3. Current knowledge about glacial evolution in Tröllaskagi Peninsula

A growing body of geochronological evidences of the deglaciation in the Tröllaskagi area, encompassing different time scales has come out in recent decades. The first works focusing on lichenometric and radiocarbon-tephrochronological dating were subsequently complemented with CRE dating based on the cosmogenic nuclide ^{36}Cl and the analysis of historical aerial photos. These data indicate that the deglaciation of the fjords and valleys started at ~16 ka, and was followed by an accelerated retreat by 12 ka (Norðdahl and Pétursson, 2005; Norðdahl et al., 2008; Pétursson et al., 2015; Andrés et al., 2019; Fernández-Fernández et al., 2019, 2020). The glacier outlet of the Icelandic Ice Sheet (IIS) that flowed down by Skagafjörður fjord rapidly retreated by 11 ka (Andrés et al., 2019). In addition, at the head of, at least, 5 valleys in the Tröllaskagi Peninsula, moraines and erratic boulders distributed very close to the present-day glacier fronts were deposited at ~11 ka (Fernández-Fernández et al., 2020). Shortly after their formation, rock glacier fronts collapsed at ~9 ka (Fernández-Fernández et al., 2020). Currently, some active rock glaciers and debris-covered glaciers (i.e. with ice cores) still survive at the bottom of many of the valley heads, but their kinematics are mostly controlled by subsidence processes (Tanarro et al., 2019; Campos et al., 2019). ^{36}Cl CRE dating of some boulders on the surface of these landforms indicates their stagnation at 7–5 ka (Fernández-Fernández et al., 2020).

During the Holocene Thermal Maximum (HTM) (10–6 ka) the debris-free glaciers, due to their high climate sensitivity, have most probably disappeared in central Iceland (Geirsdóttir et al., 2009, 2019; Larsen et al., 2012) and the nearby Langjökull and Drangajökull ice caps (Anderson et al., 2018b). The evolution of the few debris-free glaciers of Tröllaskagi during the HTM is not known. Nevertheless, there is evidence of Neoglacial glacier inception in Iceland at ~5 ka and ~2.5 ka (Langjökull and Drangajökull ice caps) and depression of their Equilibrium-Line Altitudes (ELA) in response to the summer temperature decline that started at ~5 ka (Geirsdóttir et al., 2019). From ~5 ka onwards, a series of significant advances occurred in Southern and Central Iceland (Kirkbride and Dugmore, 2006, 2008) as a consequence of the regional climate cooling (Andersen et al., 2004; Geirsdóttir et al., 2009, 2013, 2019). Neoglacial expansions of Langökull and NE Vatnajökull have been reported at 4.5–4.0 and 3 ca ka BP (Striberger et al., 2011, 2012; Geirsdóttir et al., 2019). Glacial advances have been dated also at the south and the center of the island at 2.3, 1.7 cal ka BP (Kirkbride and Dugmore, 2008), and at 5.0–4.5, 3.5–3.0 and 2.5–2.0 cal ka BP, respectively (Kirkbride and Dugmore, 2006). In Tröllaskagi, Neoglacial advances of debris-free glaciers have been dated at 4.7, 4.2, 3.2–3.0, 2.0, 1.5 and 1.0 cal ka BP (see synthesis in Stötter et al., 1999). CRE dating revealed major Neoglacial glacial culminations in Tröllaskagi at 1.6 and 1.3 ka, during the Dark Ages cold period (Helama et al., 2017; Fernández-Fernández et al., 2019).

The greatest cooling of the second half of the Holocene in Iceland occurred between 0.7 and 0.1 ka, during the LIA (Ogilvie and Jónsson, 2001; Larsen et al., 2012). At that time, the lowest Holocene temperatures were recorded, coinciding with the maximum expansion of sea ice and the stabilization or advance of glaciers (Miller et al., 2010). Icelandic glaciers started their LIA expansion in the 13th century (Larsen et al., 2011) and reached their maximum extent in the south and in the center of the island either in the 18th (Kirkbride and Dugmore, 2006, 2008) or 19th century, depending on the glaciers (Chenet et al., 2010). In Tröllaskagi, studies supported by lichenometric dating suggested that the maximum LIA expansion occurred in the late 19th or even in the early 20th century (Caseldine and Cullingford, 1981; Caseldine, 1983, 1985; Kugelmann, 1991; Häberle, 1991; Caseldine and Stotter, 1993). However, recent CRE dating in the Vesturdalur and Austurdalur valleys (central Tröllaskagi) showed that the maximum LIA expansion was reached between the 15th and 17th centuries at the latest (Fernández-Fernández et al., 2019). Several minor glacier advances or standstills occurred throughout the 19th century (decades of 1800s, 1830s, 1840s, 1860s and 1890s), in response to cold episodes of the late-LIA (Fernández-Fernández et al., 2019). Since the beginning of the 20th century, glaciers experienced a general retreating trend only interrupted by several advances in the 1910s, 1950s and from the mid-1980s to the mid-1990s (Fernández-Fernández et al., 2017, 2019).

4. Methods

4.1. Geomorphological analysis and mapping

Geomorphological mapping was the basis to identify the different phases within the deglaciation, and followed the methodology applied on previous studies conducted in Iceland (e.g. Evans et al., 2017; Tanarro et al., 2018; Fernández-Fernández and Andrés, 2018; Fernández-Fernández et al., 2019; Rodríguez-Mena et al., 2021). Mapping digitizing and design were carried out in the software MicroStation Connect, supported on stereoscopic photointerpretation and visual inspection of historical aerial photographs (Icelandic Land Survey, 2017–2020), later validated with a fieldwork in August 2018. Mapping was also supported by the analysis of orthophotos (2000 and 2019) and high-resolution digital elevation models (DEM) obtained through the application of the Structure from Motion (SfM) photogrammetric technique (Micheletti et al., 2014, 2015; Gomez et al., 2015) to 1946 and 1994 historical aerial photographs. The Bentley Context Capture photogrammetry software was also used to process the 43 terrestrial photographs of a section of the frontal area of the glacier, taken on August 30, 2018 from the opposite slope, and at a distance between 500 and 1300 m from the photographed landforms to obtain a DEM and an orthophoto, with a high resolution (0.27 m).

With the help of all these materials, the main landforms were classified into geomorphological units, and subsequently, the geometry of former glacier margins in different glacial stages was reconstructed based on the moraine ridge mapping. The current glacier margin was outlined onto an aerial photo obtained in 2019 from an online geoviewer (Icelandic Land Survey, 2017–2020).

4.2. Glacier reconstruction and equilibrium-line altitude (ELA) calculations

The palaeoglacier reconstruction was approached according to physical-based numerical procedures. As the study area is currently occupied by a glacier, we first modelled glacier bedrock topography by estimating its ice thickness distribution through the model 'VOLTA'

(Volume and Topography Automation; James and Carrivick, 2016), a Python script tool for ArcGIS 10.7.1. This tool, which only requires the glacier geometry and its DEM, can create the glacier centerline along which ice thickness is calculated based on the assumption of perfect-plasticity ice. The resulting DEM with the corrected bedrock was used to reconstruct the glacier in the previously identified glacial stages.

After that, we carried out the glacier reconstruction by using the ArcGIS toolbox 'GlaRe' (Pellitero et al., 2015, 2016) in the same work environment. This is a semi-automatic tool that implements the procedures proposed by Benn and Hulton (2010), relying on the Van der Veen (1999) equation for modeling the past ice thickness along a flowline. First, we digitized the main and tributary flowlines by hand from terminus to the headwall. To simplify the glacier reconstruction, we assumed that shear-stress remained constant along the flowline and throughout time. To achieve a realistic value, we modelled shear stress along the flowline by using the *Profiler v2* Excel™ spreadsheet of Benn and Hulton (2010) so that the modelled ice thickness matches the current glacier topography. We obtained an average value of 95 kPa, within the normal shear-stress range (50–150 kPa) and very close to the average typical 100 kPa value observed in current glaciers (Benn and Hulton, 2010). Thus, we used this value in the toolboxes contained in 'GlaRe' to reconstruct the past ice thicknesses along the flowlines. Subsequently, in order to achieve a realistic reconstruction, we adjusted the reconstructed contours so that they show the typically convex and concave pattern towards the terminus and headwall, respectively.

For ELA calculations, we used the automatic "ELA calculation" ArcGIS toolbox (Pellitero et al., 2015, 2016). We followed the AAR (Accumulation Area Ratio; Meier and Post, 1962; Porter, 1975) and AABR (Area Altitude Balance Ratio; Osmaston, 2005) methods. For the AAR method we used the ratio 0.67, previously assumed for Tröllaskagi glaciers (Stötter, 1990; Caseldine and Stotter, 1993). For the AABR method we used the ratio 1.5 ± 0.4 which has been successfully tested in Tröllaskagi (Fernández-Fernández and Andrés, 2018; Fernández-Fernández et al., 2017, 2019).

4.3. Cosmic-Ray Exposure dating methods

During the summers of 2015 and 2018, fieldworks were conducted in the Héðinsdalur valley aiming to conduct geomorphological survey and collect rock samples from the main geomorphological units in the foreland. The propose was to reconstruct the geomorphological evolution that drove the transformation of the Héðinsdalsjökull and its evolution towards the debris-covered glacier and the rock glacier.

A total of 9 samples with thicknesses of 2–5 cm were extracted from the surficial layer of moraine and rock glacier boulders (Table 1) by means of a hammer and a chisel. Stable and well-embedded boulders far from the influence of slope processes where preferred so that the potential risk of overturning is minimized. Aiming to ensure the optimal exposure to the cosmic-rays, flat and gentle rock faces were preferred to sharp crests and steep sides (always at the top of the boulders). To account for the partial shielding due to the surrounding mountains and hills, the topographic shielding factor was calculated for all the sampling sites by means of the ArcGIS toolbox devised by Li (2018). This tool which implements well-known routines explained in Dunne et al. (1999) and only needs: (i) a point shapefile of the sampling sites including the strike and the dip of the sampling surfaces and (ii) a digital elevation model. We used this method due to the impossibility of carrying out the field measurements of the horizon line with an optical clinometer due to the typical Icelandic weather (i.e. bad visibility by cloudiness).

After that, samples were crushed and sieved to the 0.25–1.0 mm fraction at the "Physical Geography Laboratory" of the Complutense University of Madrid (Spain). According to the basaltic lithology of the study area, the in situ produced cosmogenic nuclide ^{36}Cl was chosen to perform the CRE dating. As none of the samples had enough feldspar minerals, we followed chemical procedures for the ^{36}Cl extraction in whole rock, based on Schimmelpfennig et al. (2011). The chemical sample processing was conducted in the "Laboratoire National des Nucléides Cosmogéniques" (LN_2C) of the "Centre Européen de Recherché et d'Enseignement des Géosciences de l'Environnement" (CEREGE; Aix-en-Provence, France). Before the chemical processing, we took a 5-g aliquots of untreated bulk samples in order to determine the sample composition (i.e. concentration of major/trace elements; Table 2) at the "Service d'Analyse des Roches et des Minéraux" (SARM, CRPG, Nancy, France) by using ICP-OES for the major element concentrations, ICP-MS for most of the trace elements, atomic absorption for Li, colorimetry for B and spectrophotometry for Cl. Initial sample weights of 60–120 g were used, depending on the expected ages, and were rinsed with ultrapure water for 3 h aiming to remove dust and fines. Then, to remove atmospheric ^{36}Cl and potentially chlorine-rich ground mass, a ~30% of the sample mass was dissolved by leaching with a mixture of diluted nitric acid (10% HNO_3) and concentrated hydrofluoric acid (48% HF). Subsequently, the remaining etched sample mass was rinsed and dried, and 2-g aliquots were taken aiming to determine the major elements concentrations in the target fraction at SARM by ICP-OES (Table 3). Before the total dissolution of the samples, about 260 μL and 330 μL of two in-house manufactured ^{35}Cl carriers, respectively (spike 010813, 6.92 mg Cl g^{-1}, $^{35}Cl/^{37}Cl$ ratio 917.75; spike 201,018, 6.019 ± 0.115 mg Cl g^{-1}, $^{35}Cl/^{37}Cl$ ratio 296.9 ± 3.6) were added to the samples for isotopic dilution (Ivy-Ochs et al., 2004). Samples were totally dissolved, in a mixture of 9 mL 10% HNO_3 and 4.5 mL 48% HF per gram of sample, and to make it more effective, samples were shaken for 48 h. After total dissolution, samples were centrifuged aiming to separate the dissolved sample from the fluoride complexes and potentially undissolved residues. Then, 2 mL of diluted (10%) silver nitrate ($AgNO_3$) were added to precipitate the chlorine from the liquid solution as silver chloride (AgCl). Bottles with the samples were stored for 48 h in a dark place to allow the AgCl precipitate to settle down on the bottom. After that, we extracted the supernatant solution (HF + HNO_3) by using a peristaltic pump and avoiding disturbance of the precipitate. After the re-dissolution of this first AgCl precipitate, sulphur was removed as barium sulphate ($BaSO_4$), by adding 1 mL of a saturated solution of barium nitrate ($Ba(NO_3)_2$), with the aim of reducing the isobaric interferences of ^{36}S during the Accelerator Mass Spectrometer (AMS) measurements. This $BaSO_4$ was separated from the supernatant solution by filtration through an acrodisc filter. Subsequently, AgCl was precipitated again by adding 3–4 mL of diluted HNO_3 (1:1 vol.).

Table 1
Geographic sample locations, topographic shielding factor and sample thickness.

Sample name	Geomorphological unit	Latitude (DD)	Longitude (DD)	Elevation (m a.s.l.)	Topographic shielding factor	Thickness (cm)
HEDIN-1	Collapsed debris-covered glacier (CDCG)	65.6454	−18.9292	620	0.9733	3.5
HEDIN-2	Collapsed debris-covered glacier (CDCG)	65.6455	−18.9272	651	0.9753	2.0
HEDIN-3	Collapsed debris-covered glacier (CDCG)	65.6455	−18.9278	640	0.9756	2.5
HEDIN-4	Rock glacier (RG)	65.6399	−18.8925	960	0.9903	4.3
HEDIN-5	Rock glacier (RG)	65.6397	−18.8922	962	0.9892	3.7
HEDIN-6	Rock glacier (RG)	65.6392	−18.8911	971	0.9646	5.0
HEDIN-7	Moraine (M)	65.6406	−18.8993	974	0.9942	3.5
HEDIN-8	Moraine (M)	65.6407	−18.8994	974	0.9762	3.8
HEDIN-9	Moraine (M)	65.6407	−18.8995	974	0.9934	2.8

Table 2
Chemical composition of the bulk rock samples before chemical treatment.

Sample name	CaO (%)	K_2O (%)	TiO_2 (%)	Fe_2O_3 (%)	Cl (ppm)	SiO_2 (%)	Na_2O (%)	MgO (%)	Al_2O_3 (%)	MnO (%)	P_2O_5 (%)	Li (ppm)	B (ppm)	Sm (ppm)	Gd (ppm)	Th (ppm)	U (ppm)
Collapsed debris-covered glacier																	
HEDIN-1	10.773	0.262	2.880	14.920	40	47.290	2.282	6.423	12.918	0.213	0.240	4.4	2.000	5.447	5.704	1.143	0.317
Rock glacier																	
HEDIN-4	9.937	0.415	2.970	16.070	58	48.470	2.848	5.768	12.872	0.227	0.250	5.190	3.6	6.018	6.279	1.138	0.324
HEDIN-6	10.923	0.358	2.671	14.320	44	48.280	2.703	6.286	13.942	0.201	0.250	5.500	2.000	5.769	6.069	1.057	0.291
Average	10.430	0.387	2.821	15.195	51	48.375	2.776	6.027	13.407	0.214	0.250	5.345	2.000	5.894	6.174	1.098	0.307
Moraine																	
HEDIN-8	11.600	0.301	2.593	13.805	34	47.140	2.340	7.782	13.492	0.192	0.240	4.260	2.000	5.230	5.432	1.106	0.286

Table 3
Concentrations of the ^{36}Cl target elements (Ca, K, Ti and Fe) and other major elements (Si, Al, Mn, Mg and Na) determined in splits taken after the chemical pre-treatment (acid etching).

Sample name	CaO (%)	K_2O (%)	TiO_2 (%)	Fe_2O_3 (%)	SiO_2 (%)	Al_2O_3 (%)	MnO (%)	MgO (%)	Na_2O (%)
Collapsed debris-covered glacier									
HEDIN-1	10.28 ± 0.21	0.18 ± 0.03	3.70 ± 0.18	16.91 ± 0.34	48.73 ± 0.49	9.32 ± 0.93	0.24 ± 0.01	7.32 ± 0.15	1.73 ± 0.26
HEDIN-2	7.87 ± 0.16	0.80 ± 0.04	2.65 ± 0.13	13.36 ± 0.27	55.18 ± 0.55	10.14 ± 0.10	0.20 ± 0.01	5.50 ± 0.11	2.32 ± 0.35
HEDIN-3	8.06 ± 0.16	0.76 ± 0.04	3.05 ± 0.15	14.5 ± 0.29	54.46 ± 0.54	9.73 ± 0.97	0.21 ± 0.01	5.83 ± 0.12	2.20 ± 0.33
Rock glacier									
HEDIN-4	9.45 ± 0.47	0.41 ± 0.10	3.48 ± 0.35	15.31 ± 0.31	51.39 ± 1.03	10.65 ± 0.21	0.23 ± 0.05	5.79 ± 0.12	2.46 ± 0.25
HEDIN-5	9.95 ± 0.50	0.39 ± 0.10	3.82 ± 0.38	16.68 ± 0.33	48.89 ± 0.98	11.19 ± 0.22	0.23 ± 0.05	5.90 ± 0.12	2.36 ± 0.24
HEDIN-6	9.95 ± 0.50	0.35 ± 0.09	2.95 ± 0.29	14.23 ± 0.28	51.38 ± 1.03	10.98 ± 0.22	0.20 ± 0.04	6.46 ± 0.13	2.21 ± 0.22
Moraine									
HEDIN-7	8.88 ± 0.44	0.39 ± 0.10	3.74 ± 0.37	18.03 ± 0.36	49.9 ± 1.00	9.29 ± 0.93	0.24 ± 0.05	6.19 ± 0.12	2.01 ± 0.20
HEDIN-8	10.85 ± 0.22	0.27 ± 0.07	3.01 ± 0.30	14.39 ± 0.29	49.68 ± 0.99	9.95 ± 1.00	0.19 ± 0.04	8.14 ± 0.16	1.8 ± 0.18
HEDIN-9	11.11 ± 0.22	0.23 ± 0.06	3.05 ± 0.31	14.61 ± 0.29	49.38 ± 0.99	9.45 ± 0.95	0.20 ± 0.04	8.57 ± 0.17	1.71 ± 0.17

Finally, the precipitate centrifuged, rinsed and dried in the oven at 80 °C for 48 h.

Final AgCl targets were analysed at the AMS facility "Accélérateur pour les Sciences de la Terre, Environnement et Risques" (ASTER) at CEREGE, to measure the specific isotope ratios $^{35}Cl/^{37}Cl$ and $^{36}Cl/^{35}Cl$ from which the ^{36}Cl concentrations were inferred (Table 4). The measurement of these ratios was normalized to the in-house standard SM-CL-12 with an assigned $^{36}Cl/^{35}Cl$ ratio value of (1.428 ± 0.021) 10^{-12} (Merchel et al., 2011) and assuming a natural ratio of $^{35}Cl/^{37}Cl$ = 3.127. Analytical 1σ uncertainties include AMS counting statistics and the external machine stability (Braucher et al., 2018).

^{36}Cl exposure ages were calculated in the Excel™ spreadsheet for in-situ calculations proposed by Schimmelpfennig et al. (2009) as it allows the input of specific ^{36}Cl production rates. The used ^{36}Cl production rates – referenced to sea level and high latitude (SLHL) – were from spallation of Ca, K, Ti and Fe: 57.3 ± 5.2 ^{36}Cl (g Ca)$^{-1}$ yr^{-1} (Licciardi et al., 2008), 148.1 ± 7.8 ^{36}Cl (g K)$^{-1}$ yr^{-1} (Schimmelpfennig et al., 2014), 13 ± 3 ^{36}Cl (g Ti)$^{-1}$ yr^{-1} (Fink et al., 2000) and 1.9 ± 0.2 atoms ^{36}Cl (g Fe)$^{-1}$ yr^{-1} (Stone et al., 2005), respectively. The elevation-latitude scaling factors were based on the time invariant scheme ("St"; Stone, 2000). The production rate used for epithermal neutrons for fast neutron in the atmosphere at the land/atmosphere

Table 4
AMS analytical data and calculated exposure ages. $^{36}Cl/^{35}Cl$ and $^{35}Cl/^{37}Cl$ ratios were inferred from measurements at the ASTER AMS facility. The numbers in brackets correspond to the internal (analytical) uncertainty at 1σ deviation.

Sample name	Sample weight (g)	mass of Cl in spike (mg)	$^{35}Cl/^{37}Cl$	$^{36}Cl/^{35}Cl$ (10^{-14})	[Cl] in sample (ppm)	[^{36}Cl] (10^4 atoms g^{-1})	Age (ka)
Collapsed debris-covered glacier							
HEDIN-1	67.56	1.878	8.846 ± 0.085	4.531 ± 0.258	19.9	3.167 ± 0.202	2.8 ± 0.3 (0.2)
HEDIN-2	64.38	1.875	4.706 ± 0.045	2.523 ± 0.165	76.5	3.571 ± 0.286	2.4 ± 0.3 (0.3)
HEDIN-3	63.98	1.893	4.717 ± 0.044	2.207 ± 0.157	77.1	3.136 ± 0.269	2.1 ± 0.3 (0.2)
Rock glacier							
HEDIN-4	81.14	1.824	5.038 ± 0.100	10.694 ± 0.758	47.9	10.74 ± 1.126	6.3 ± 0.9 (0.8)
HEDIN-5	84.98	1.811	5.427 ± 0.094	3.067 ± 0.309	37.6	2.597 ± 0.32	1.5 ± 0.2 (0.2)
HEDIN-6	84.05	1.796	6.758 ± 0.122	1.531 ± 0.235	23.7	1.012 ± 0.169	0.6 ± 0.1 (0.1)
Moraine							
HEDIN-7	40.46	1.829	9.900 ± 0.176	8.683 ± 0.575	26.6	9.698 ± 0.734	6.4 ± 0.8 (0.7)
HEDIN-8	41.02	1.815	20.442 ± 0.444	4.390 ± 0.391	9.6	3.850 ± 0.354	2.6 ± 0.3 (0.3)
HEDIN-9	42.11	1.813	24.322 ± 0.465	12.734 ± 1.518	7.5	10.640 ± 1.282	7.0 ± 1.1 (1.0)

Blanks					Total atoms Cl (10^{17})	Total atoms ^{36}Cl (10^4)	
BK-1[a,b]	–	1.888	328.059 ± 2.892	0.359 ± 0.069	2.65 ± 0.136	11.725 ± 2.249	–
BK-2	–	1.821	202.688 ± 6.266	0.057 ± 0.028	2.051 ± 0.306	1.776 ± 0.891	–
BK-3	–	1.805	153.865 ± 3.733	0.058 ± 0.022	4.086 ± 0.507	1.823 ± 0.692	–

[a] The ^{35}Cl carrier (spike) added to the samples HEDIN 1–3 and BK-1 was 010813(4): [Cl] = 6.92 mg Cl g^{-1}. $^{35}Cl/^{37}Cl$ ratio = 917.75. To the rest of the samples, BK-2 and BK-3 the spike added was 261,018: [Cl] = 6.019 ± 0.115 mg Cl g^{-1}. $^{35}Cl/^{37}Cl$ ratio = 296.9 ± 3.6.

[b] In parallel to the sample treatment, three blanks were prepared: BK-1 (processed with: HEDIN 1–3 samples), BK-2 (processed with samples HEDIN 7–9) and BK-3 (processed with sample HEDIN 4–6).

interface was 696 ± 185 neutrons (g air)$^{-1}$ yr^{-1} (Marrero et al., 2016). The high energy neutron attenuation length applied was 160 g cm^{-2}.

Iceland is permanently affected by the Icelandic Low (note that the average sea-level pressure in Akureyri is 1006.9 hPa and not the standard 1013.25 hPa). As the atmospheric pressure modifies the cosmic-

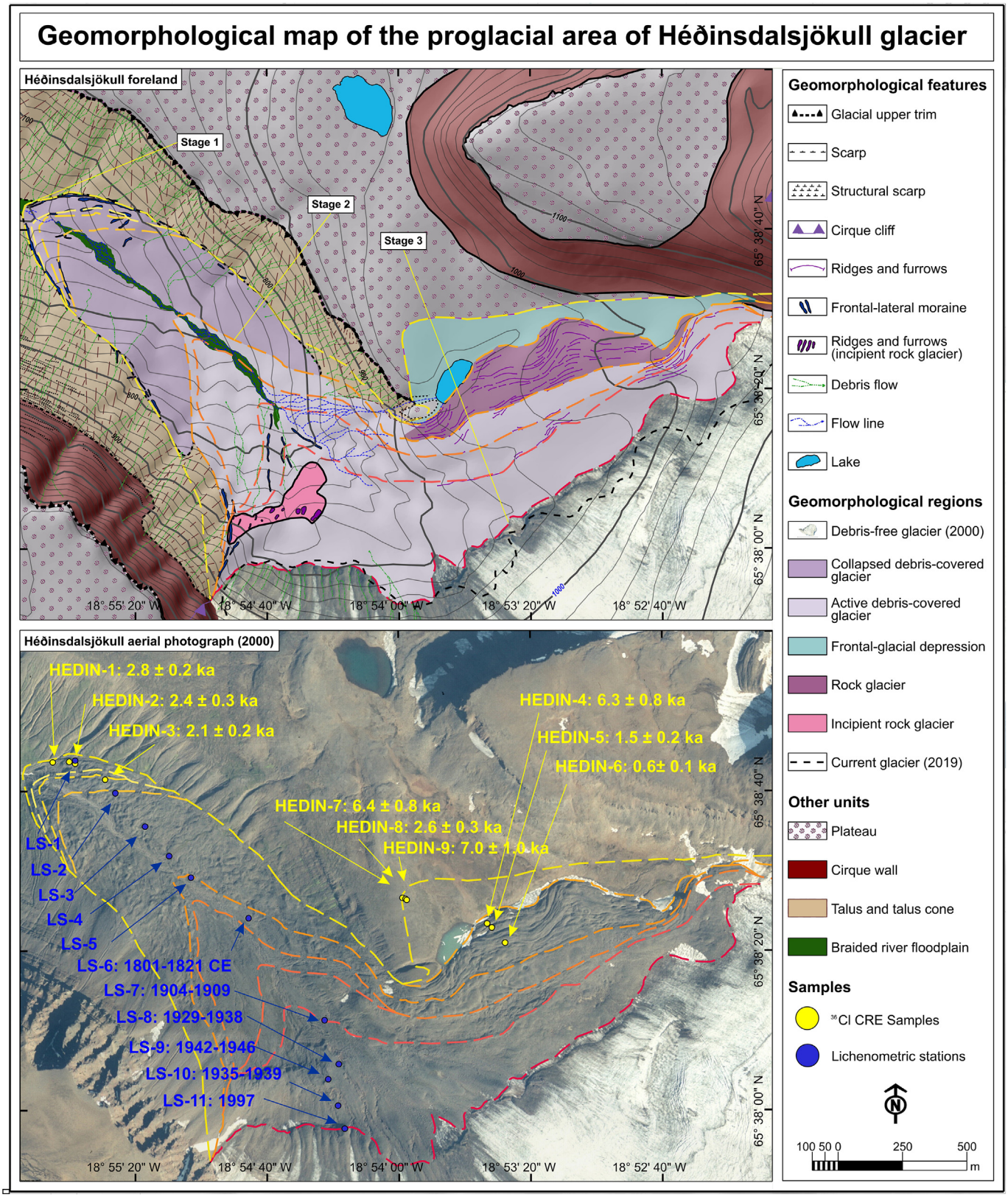

Fig. 2. Geomorphological units of Héðinsdalsjökull glacier. A) Geomorphological map of Héðinsdalsjökull glacier with the inferred geometry of the main stages within the glacial evolution. B) Overhead view of the Héðinsdalsjökull glacier complex and location of ^{36}Cl CRE sampling sites and LS, with their ages (expressed in ka and CE years, respectively) over the ortophoto of 2000.

ray particle flux and thus has an impact on the local cosmogenic nuclide production rate, the atmospheric pressure anomaly was taken into account when scaling the SLHL production rates to the sampling sites. For this reason, the ERA40 atmosphere model (Uppala et al., 2005) was used to calculate elevation-latitude scaling factors. As the Licciardi et al.'s (2008) production rate already accounts for this air pressure anomaly and the calibration sites are located in south western Iceland (see also Licciardi et al., 2006), this production rate was preferred to other calibrated elsewhere (e.g. Stone et al., 1996; Schimmelpfennig et al., 2011; Marrero et al., 2016).

Uncertainties in the presented exposure ages include the uncertainties in the AMS measurements (analytical uncertainty; 1σ) and those derived from the production rate uncertainties (Table 4) unless otherwise is stated. No erosion or snow correction has been applied for the age calculations.

4.4. Lichenometric dating

To estimate the minimum stabilization age of the boulders on the surface of the collapsed and active sectors of the debris-covered glacier, two transects were followed along which we stablished a number of lichen stations (LS hereafter) (Fig. 2). In each transect, we selected the most stable boulders, always in the sharpest and most prominent ridges, so that the impact of snow cover on lichen colonization and growth is minimized. The transects were traced from the most distal sectors of the glacier to the head of the glacier and, in each case, sampling was started from areas without coalescing thalli and continued until no lichen was found. Due to time constraints, at each lichen station the largest *Rhizocarpon geographicum* and *Porpidia* cf. *soredizodes* thalli (according to their longest axis) were searched visually within a maximum 10-m radius. Circular- or ellipsoidal-shaped thalli located on smooth horizontal boulder surfaces were preferred (Innes, 1985). They were subsequently measured in-situ, retaining only the single largest one for each station. A more accurate measurement was made later from high-resolution digital photographs taken in "macro" mode with a graphic scale: each thallus was scaled to real size and measured in the ArcMap environment (see Fernández-Fernández et al., 2019). Finally, lichen-derived ages of the *Rhizocarpon geographicum* and *Porpidia* cf. *soredizodes* species were calculated by applying growth rates of 0.44 mm yr^{-1} (Kugelmann, 1991) and 0.737 mm yr^{-1} (Fernández-Fernández et al., 2019). These growth rates represent average values for surface exposed areas <160–200 years in northern Iceland considering the linear growth phase (Innes, 1985; Bradwell, 2001). Both rates are considered appropriate as they have been obtained in nearby valleys, similar to Héðinsdalur in terms of climate and geomorphological settings. The assumed colonization lags for *Rhizocarpon geographicum* and *Porpidia soredizodes* are 20 and 10 years, respectively (see Fernández-Fernández et al., 2019).

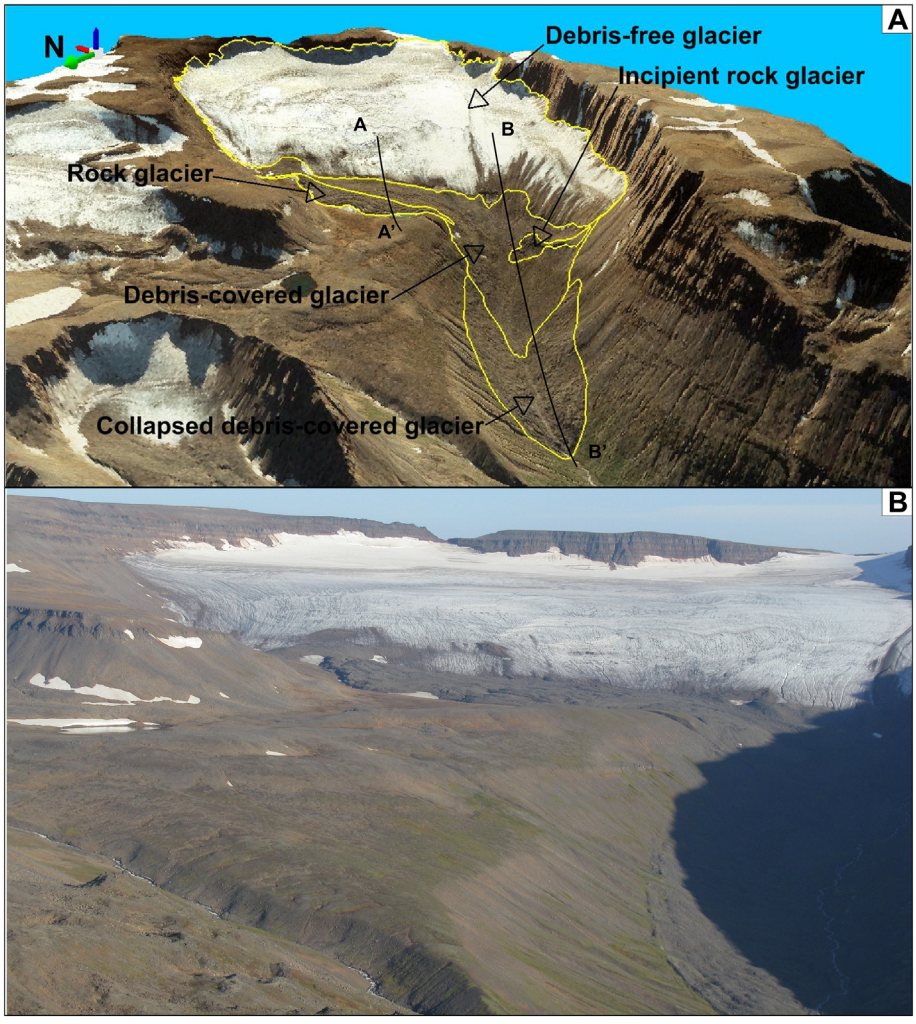

Fig. 3. A) 3D oblique view of the Héðinsdalsjökull glacier derived from the reconstructed orthophoto from 2000. Note that the three main stages and the transects A-A' and B-B′ of the Fig. 5 are outlined. B) Panoramic view (from the east) of the Héðinsdalsjökull glacier in 2018.

5. Results

5.1. Geomorphological setting

The foreland area of Héðinsdalsjökull is divided into two sectors: (A) the higher one rests on a plateau at 950–1000 m to the NE of the glacier; and (B) the lower one is located at the bottom of the valley, at 600 m, to the NW of the glacier (Figs. 2, 3). In each sector, three glacial stages were identified and outlined: Stage 1 refers to the maximum extent of the studied glacial landforms, although the outermost glacial landforms may be of a different age in each sector; Stage 2 is defined by a well-preserved moraine ridge, and Stage 3 refers to the limit of the glacier in 2000 (Fig. 2B).

A) In the sector resting on the plateau up to 5 main geomorphological units were differentiated (Figs. 2A, 4, 5A, 6, 7, 8), namely:

a.1) A *line of moraine boulders* deposited by a debris-free glacier, limiting the outer edge of a frontal-glacial depression (Figs. 6, 7A).

a.2) "*Frontal-glacial depression*" located between the moraine and the rock glacier and is occupied by a lake (Figs. 6A, 7A).

a.3) *Rock glacier* (active) with an ice core at present (according with observation in collapsed depressions) (0.2 km^2, maximum width and length of 1.2 km and 245 m, respectively) advances over the depression and the lake both in the collapsed and active zone (Figs. 6, 7). The rock glacier initiates at 1020 m and descends to 920 m with an average slope of 10.9%. It shows the typical morphology constituted by a steep front and an alternation of parallel ridges and furrows, perpendicular to the flow. Only a few collapse depressions were found on the surface, where we could observe the debris and their internal interstitial ice.

a.4) The frontal moraine of a *debris-covered glacier* overlaps the rock glacier (Stage 2). The glacier is still preserved under the debris-cover,

Fig. 4. A) Hummocky moraines and flat-bottomed collapse depressions on the bedrock in the collapsed debris-covered glacier, viewed from the east in 2018. B) Hummocky ice-cored moraines and collapse depressions in the active debris-covered glacier, viewed from the northeast in 2018.

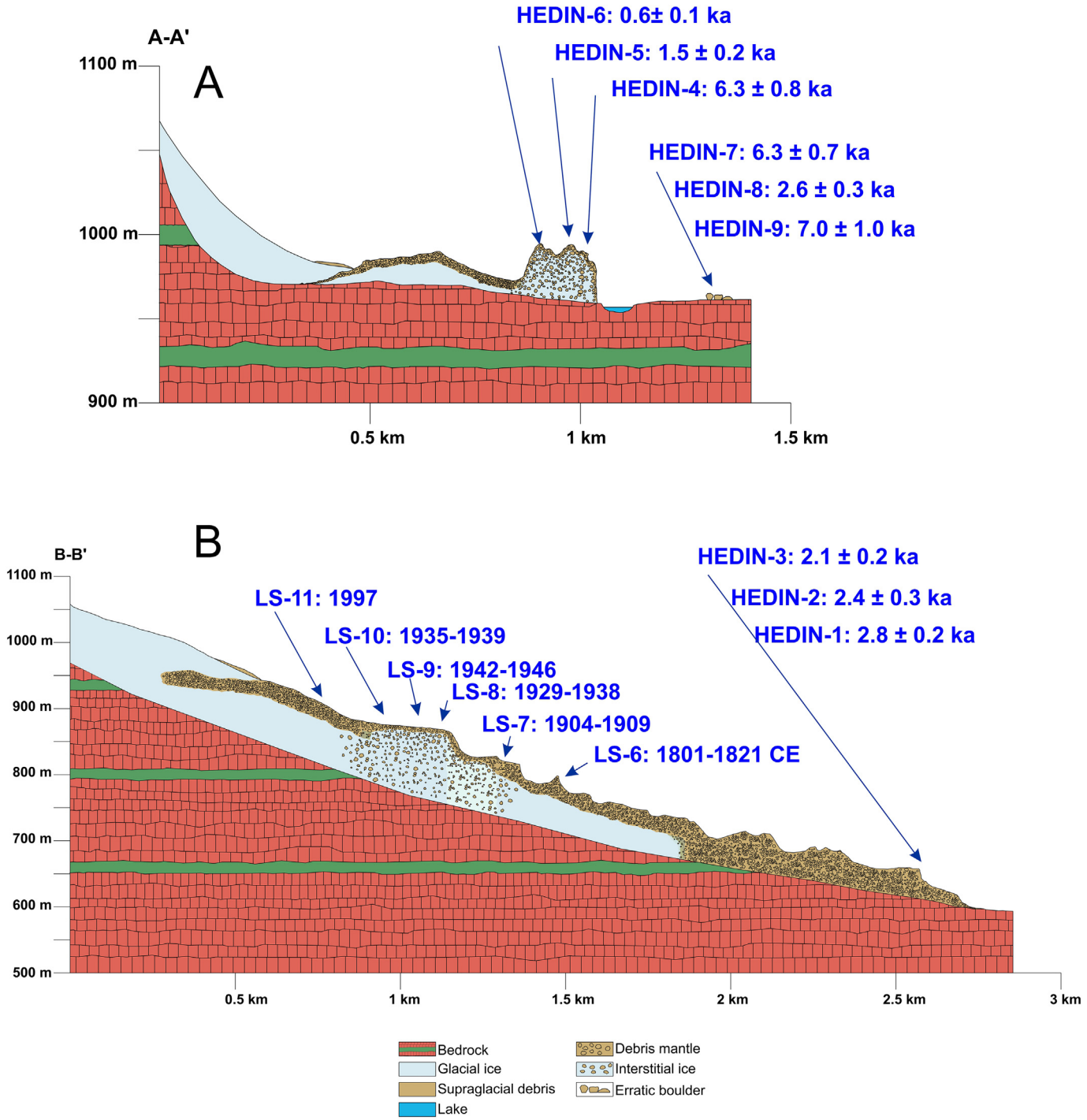

Fig. 5. A) Transect over the northern sector of the Héðinsdalsjökull glacier on the platform (see location in Fig. 3A). B) Transect on the central sector of the Héðinsdalsjökull (see location in Fig. 3A). The location of CRE samples and LS and their age/date results are given in both transects. The location of the transects is given in the Fig. 3A.

which can be observed in the collapsed depressions (Fig. 4), but has undergone an intense ice melting process as its thickness has decreased at least 10 m relative to the location of its frontal moraines located on the upper surface of the rock glacier. At least two other frontal moraine ridges are distributed in the middle of the debris-covered glacier. Minor fusion and collapse depressions (with vertical walls) are abundant on the surface showing a 0.5–1 m thick supraglacial debris mantle.

a.5) Present-day *debris-free glacier* (Stage 3), overlapping the debris-covered glacier and only covered by scattered debris on its front (Fig. 3).

B) In the lower sector, at the valley bottom, four main geomorphological units are differentiated (Figs. 4, 5B, 8A, 9A, B):

b.1) *Collapsed debris-covered glacier* (without inner ice at present) (Stage 1). It covers the lower sector of Héðinsdalsjökull complex (Figs. 2, 3) and is currently collapsed due to the complete melting of the underlying ice, according with observations in collapsed depressions, where the bedrock is visible at the bottom. The upper part starts at 820 m and descends to 600 m in the former frontal area, where four terminal moraines were identified. Most of its surface morphology is characterized by hummocky

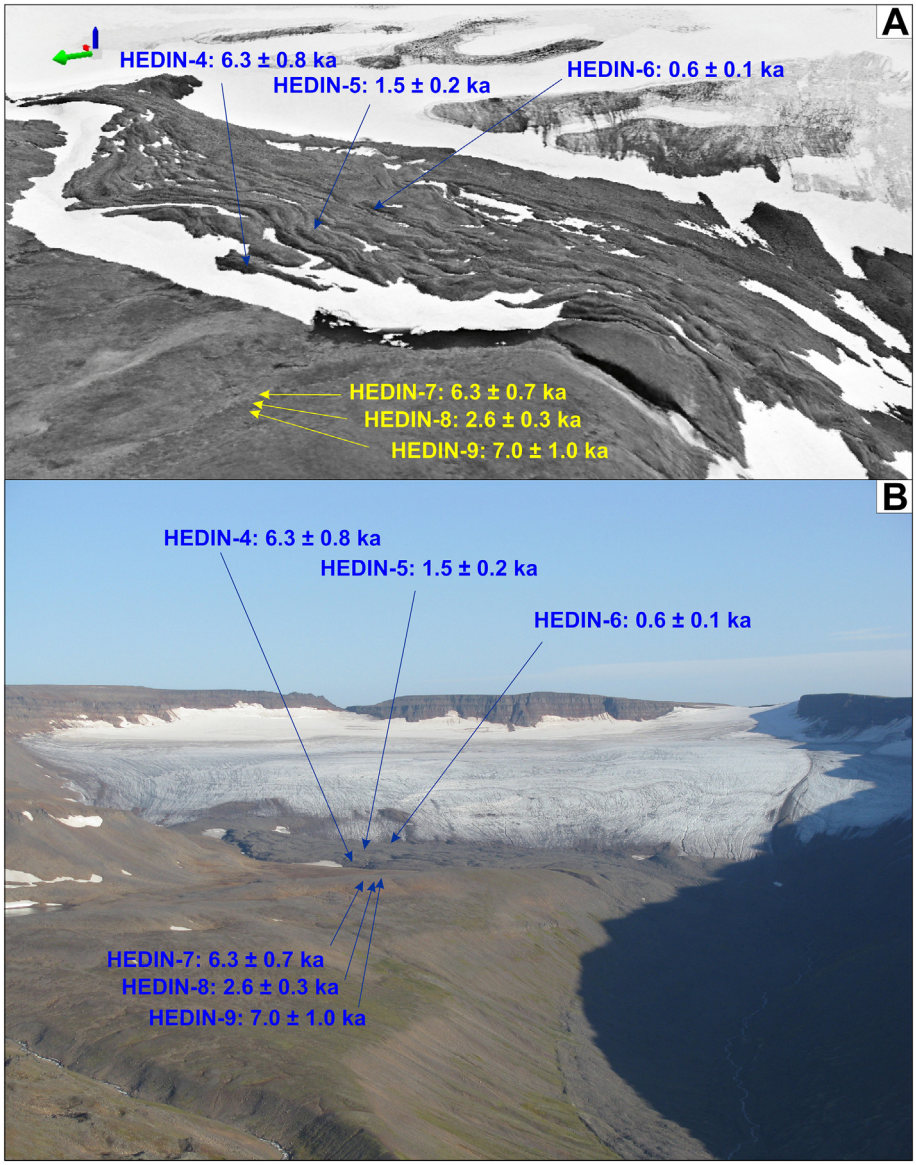

Fig. 6. A) High-resolution orthophoto (1994) of the northern sector of the Héðinsdalsjökull glacier on the platform (from the east) obtained through SfM. B) Panoramic view (from the east) of the northern sector of the Héðinsdalsjökull glacier in 2018. The location and exposure ages (ka) of the CRE samples are indicated in both panels.

moraines and flat-bottom collapse depressions over the bedrock (Fig. 4A).

b.2) *The active debris-covered glacier* (inner ice is present) (Stage 2). This glacier sector is a continuation of the unit a.4. The frontal moraine of this glacier sector overlapped the collapsed debris-covered glacier. Three more frontal moraines are located in the middle of this active debris-covered glacier, which extends over 1.2 km^2 between 1080 and 700 m. The surface morphology of this glacier is a chaotic alternation of mounds, small moraine hills and fusion depressions, of kettle hole type, some of them with vertical walls and even water-saturated, forming seasonal lagoons during the summer. Many of these depressions reveal a 0.5–1.5 m-thick supraglacial debris cover (Fig. 4B).

b.3) "*Present debris-free glacier*" (Stage 3), which follows the unit a.5 and is covered by scattered debris mainly in the western front in this sector. This debris-free glacier left a frontal moraine in the past, which overlapped the upper area of the active debris-covered glacier. The current debris-free glacier has in total an area of 4.7 km^2, and is over 2 km long and wide. The most intense retreat from the frontal moraine was recorded in its central-eastern sector, just where the scattered debris cover disappears.

b.4) *Incipient-rock glacier*. It is located in the front of the debris-free glacier, between 850 and 900 m, and is characterized by a steep front and the predominance of ridges and furrows parallel to each other and perpendicular to the flow (Fig. 10). We interpret it as an incipient rock glacier based on the small size of the features and its location within the slope. The aerial photo of 1946 shows evidence that this sector was an active frontal push moraine at that time. Therefore, we hypothesize that it constitutes a rock glacier that derived from an ice-cored moraine originated at around 1940s–1950s.

An active rock fall talus leans on the southern cirque walls and in the lower northern plain, both crossed by numerous debris flows. The distal parts of the talus and the debris flows supply sediments directly onto the debris-covered glacier.

5.2. Glacier reconstruction and ELA results

The spatial reconstruction of past glacial stages can only be done on glacier forelands with well-preserved frontal moraines or the well-known limits of the debris-free glacier. This was possible only for the outermost moraine of the collapsed debris-covered glacier

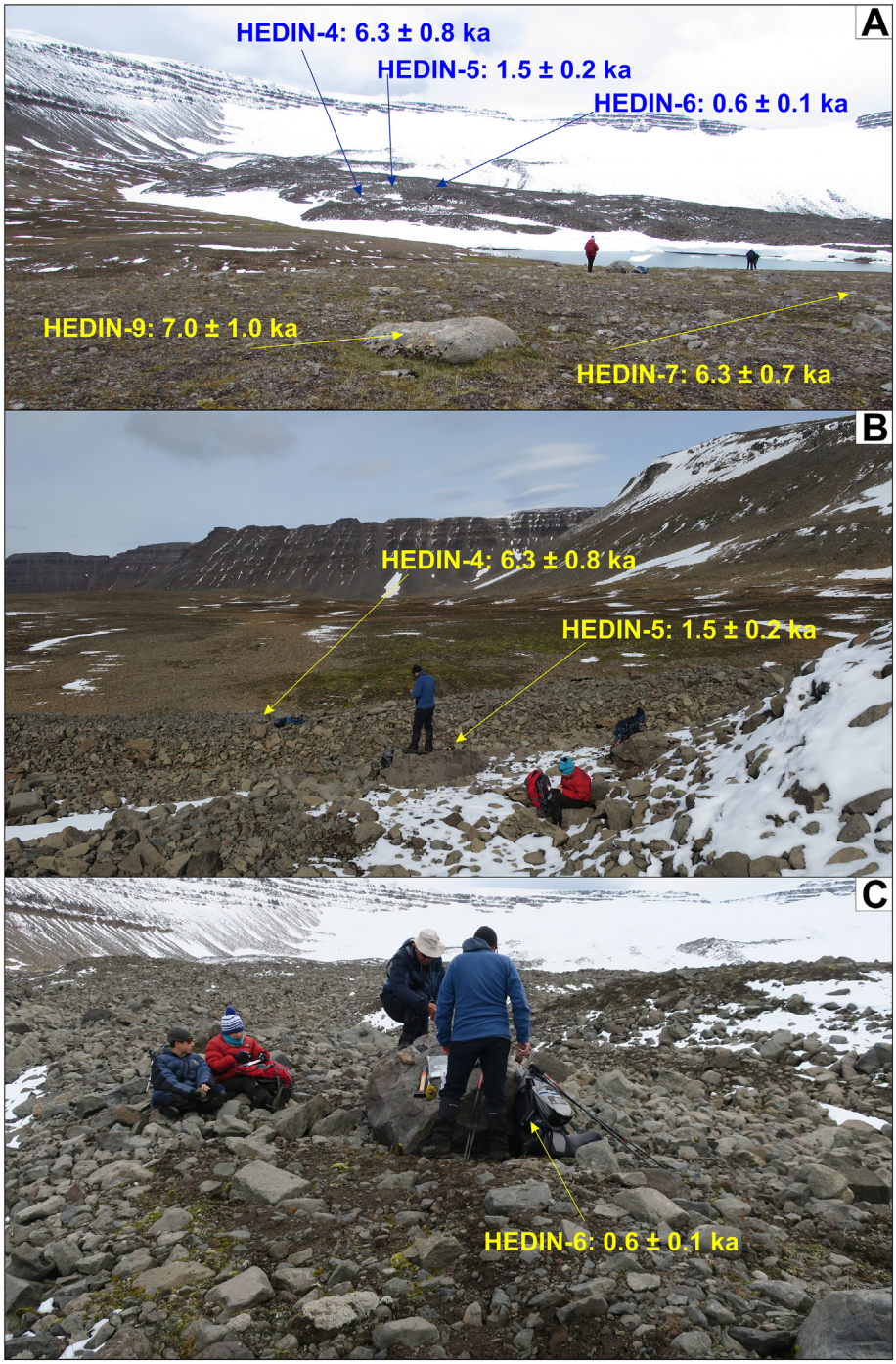

Fig. 7. A) Moraine delimiting the frontal-glacial depression and rock glacier front of the northern sector of the Héðinsdalsjökull glacier on the platform, viewed from the east (2018). B) Rock glacier front of the northern sector of the Héðinsdalsjökull glacier on the platform viewed from the south (2018). C) Roots of the rock glacier of the northern sector of the Héðinsdalsjökull glacier on the platform viewed from the east (2018). The location and results of the CRE samples are indicated in all panels.

(Stage 1), the outermost moraine of the active debris-covered glacier (Stage 2) and for the years 1946, 2000 and 2019 which best show the glacier margin geometry, which allowed to accurately outline the glacier margins (Fig. 3). During the maximum ice extent, the glacier reached a length of 5.2 km, occupied an area of 6.6 km^2 and stored 7.2 km^3 of ice. Length, extent and volume of the glacier for the remaining stages is summarized in Table 5 and Fig. 11. We calculated the ELA for these years, which revealed an elevation shift from 1042 to 1104 m (AAR method) or from 1062 to 1119 m (AABR method) (Table 5). Assuming constant precipitation for every stage and a 0.66 °C 100 m^{-1} air temperature lapse rate (Stötter et al., 1999; Fernández-Fernández et al., 2017), this ELA rise would account for a warming of 0.38 or 0.41 °C (depending on the abovementioned methods) for the whole period.

5.3. Cosmic-Ray Exposure dating

Aiming to constrain the timing of the main mapped landforms, a total of 9 samples were collected. Three of the samples (HEDIN-1, 2 and 3), previously discussed in Fernández-Fernández et al. (2020), were collected from the outermost moraine located at the front of the collapsed debris-covered glacier (Figs. 2B, 5B, 9). Their exposure ages

Fig. 8. A) Frontal moraines and collapse depressions in the collapsed debris-covered glacier viewed from the northeast in 2018. B) Rock glacier front of the northern sector of the Héðinsdalsjökull glacier on the platform, viewed from the south in 2018. The location and exposure ages of the CRE samples are indicated in both panels.

were recalculated yielding ages of 2.8 ± 0.2; 2.4 ± 0.3 and 2.1 ± 0.2 ka respectively, with an arithmetic mean of 2.4 ± 0.4 ka.

The rock glacier located on the eastern upper platform was targeted following a transect from the front to its source area (Figs. 2, 5A, 6, 7, 8B). The first sample (HEDIN-4) was taken from a boulder of the outermost ridge at 50 m from the external limit of the rock glacier, giving an age of 6.3 ± 0.8 ka. Another sample was taken from a boulder in another ridge at 50 m from the distal edge of the rock glacier (HEDIN-5), resulting in an age of 1.5 ± 0.2 ka. The last sample of this geomorphological unit was taken from a boulder at 50 m from the external limit of the rock glacier (HEDIN-6), which gave an age of 0.6 ± 0.1 ka.

Moreover, three moraine boulders were sampled on the outer distal border of the frontal-glacial depression, in front of the rock glacier, HEDIN-7, 8 and 9, which yielded exposure ages of 6.4 ± 0.7, 2.6 ± 0.3 and 7.0 ± 1.1 ka, respectively. The chi-squared test identified the sample HEDIN-8 as a potential outlier. If the age of this sample is rejected, the remaining two yield a mean age of 6.6 ± 1.0 ka.

5.4. Lichenometric results

At LS-1 to 5, located in the collapsed debris-covered glacier, and LS-6, on the outermost frontal moraine of the active debris-covered glacier, thalli coalescence was prevailing, so no lichen was measured in any of the stations (Table 6 and Fig. 2). It has been hypothesized that this circumstance occurs in Iceland on stable surfaces exposed more than 160–200 years ago according to the literature (see Maizels and Dugmore, 1985; Thompson and Jones, 1986; Evans et al., 1999). From LS-7 onwards, individual thalli were observed and measured (Table 6 and Fig. 10). According to the lichens measured in LS-7, located on an internal frontal moraine of the active debris-covered glacier, this moraine was abandoned by the glacier between 1811 and 1821 CE. The thalli

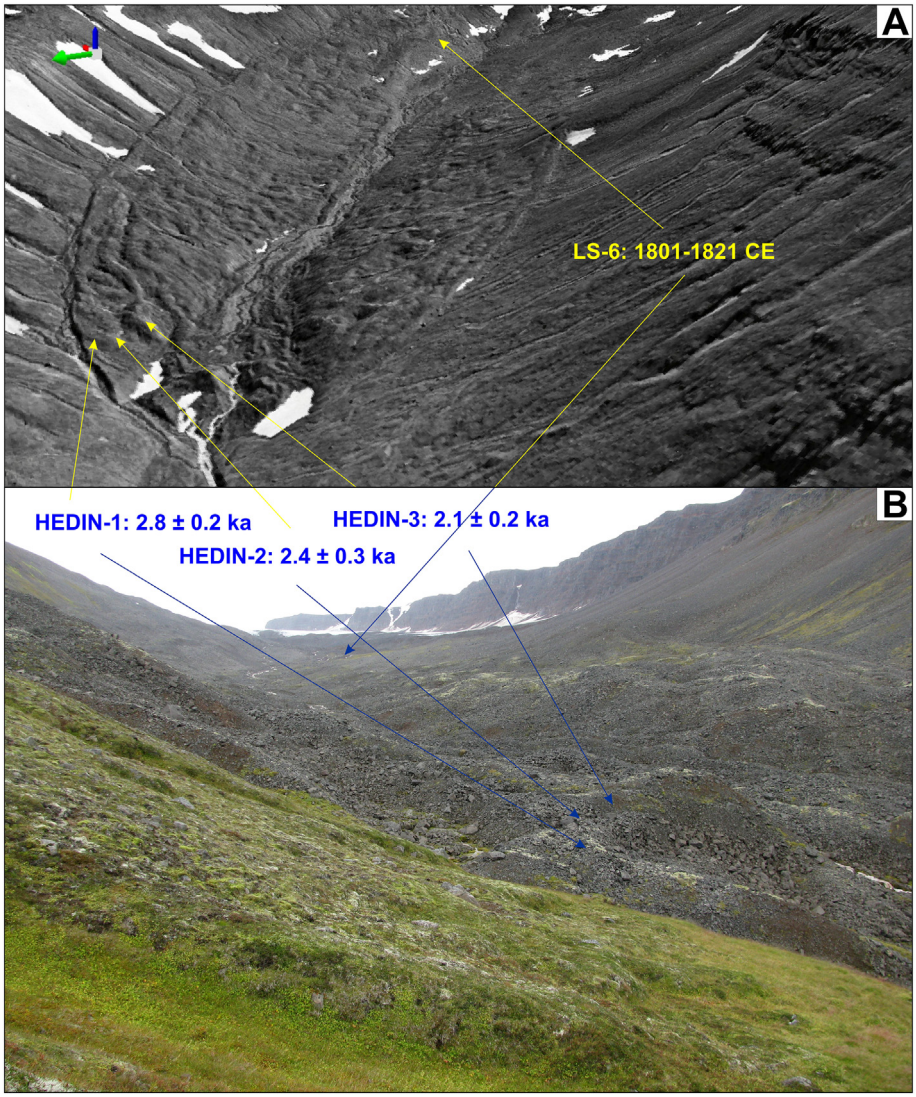

Fig. 9. A) High-resolution orthophoto (1994) (viewed from the east) of the collapsed debris-covered glacier, obtained through SfM. B) Frontal moraines and collapse depressions in the collapsed debris-covered glacier viewed from the northeast (2018). The location and exposure ages (in ka) of the CRE samples are indicated in both panels.

measurements carried out in LS-8, located on the innermost frontal moraine of the active debris-covered glacier, yielded a date of moraine abandonment between 1904 and 1919 CE. The LS-9, 10 and 11, located on what appeared to be an ice-core push moraine in the photo of 1946, dates from 1935 to 1946 CE. Finally, the LS-12, located on the moraine deposits corresponding to the position of the terminus in 2000, gave a very close date of 1997.

6. Discussion

6.1. Evolution of Héðinsdalsjökull

The combined results from geomorphological mapping, glacier reconstruction of former stages, CRE and lichenometric dating allowed to define the following phases within the complex glacial evolution of the Héðinsdalsjökull glacier:

(i) *Debris-free glacier* (Figs. 12A and 13A). The deglaciation of the valleys north of Héðinsdalur, the Hóladalur and Hofsdalur, is known to have started at 16 ka (Fernández-Fernández et al., 2019, 2020). Therefore, it is reasonable to conclude that this age might also correspond to the onset of the deglaciation of the Héðinsdalur valley. No remnants of glacial landforms were found outside the Héðinsdalsjökull foreland, which might be due to the abrupt glacial retreat, without any standstill during the deglaciation. The other possibility is that the intensive landslide and rock fall activity on the valley slopes might have covered potential geomorphical evidence of past glaciations. According to the CRE dating, the oldest glacial landforms in this valley correspond to a line of moraine boulders that delimit the outer sector of the frontal-glacial depression on the platform, in front of a the rock glacier, which yielded a mean age of 6.6 ± 1.0 ka (Fig. 12B). This simple line of boulders is considered to have been generated by a debris-free glacier, as no evidence of supraglacial debris-mantle was observed. Therefore, this age is indicative of the onset of the retreat of Héðinsdalsjökull as a debris-free one.

(ii) *Active rock glacier*. Following the retreat of the debris-free glacier, a rock glacier was formed on the platform (Fig. 12B, C). CRE ages show stabilization of its forehead at 6.3 ± 0.9 ka. The activity (flow) of this rock glacier persisted in its sector near the valley head much longer (from to 1.5 ± 0.2 ka, and finally to 0.6 ± 0.1 ka). We use the term "stabilization" along the discussion to refer to the moment when boulder stopped flowing and, thus the same rock surface was exposed uninterruptedly to radiation (Fernández-Fernández et al., 2020). The similar ages of the rock glacier front (6.3 ± 0.9 ka) and the moraine ahead

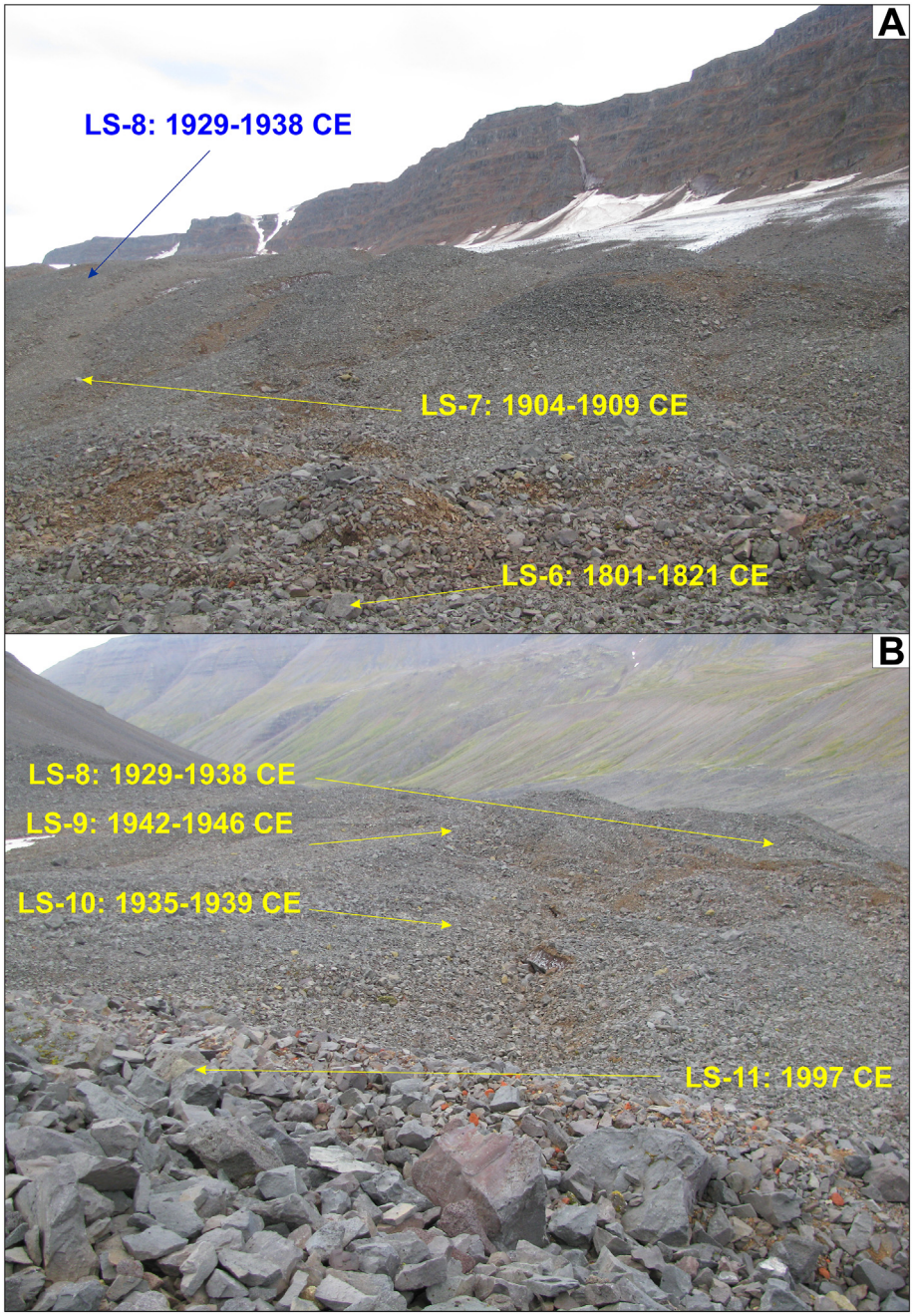

Fig. 10. The proto-rock glacier at the top of the active debris covered glacier, close to the current front of the Héðinsdalsjökull glacier. A) Frontal area of the proto-rock glacier from the east in 2018. B) Root area of the proto-rock glacier viewed from the west. The location and dates (in CE years) of the LS are indicated in all panels.

Table 5
Glacier longitude, expanse and volume calculated from reconstructions. Delta (Δ) is referred to the change regarding the stage 1 (maximum) and ELA calculations using AAR and AABR methods.

	Stage 1	Stage 2	1946	2000	2019
Length of glacier (km)	5.15	4.44	3.29	3.27	3.24
Δ (%)	–	−13.79	−36.12	−36.51	−37.09
Area (km^2)	6.98	6.04	5.15	4.92	4.67
Δ (%)	–	−13.47	−26.22	−29.52	−29.67
Vol. (km^3)	7.16	6.63	5.72	5.54	5.22
Δ (%)	–	−7.4	−20.11	−22.63	−27.09
ELA AAR (0,67; m a.s.l.)	1042	1059	1085	1095	1104
ELA AABR (1,5 ± 0,4; m a.s.l.)	1062	1089	1110	1115	1119

(6.6 ± 1.0 ka) can be explained either by the rock glacier stabilizing shortly after the moraine was abandoned, or by the boulders of the rock glacier front deriving from the moraine and retaining some nuclide inheritance (Çiner et al., 2017).

(iii) *Debris-covered glacier and its collapse*. While a rock glacier was developing and afterwards stabilizing at the glacier front located at about 900 m of altitude on the platform, a debris-covered glacier was formed in the valley bottom fed also by intense debris supplied by the western slope (Fig. 13B). CRE ages of the frontal moraine at 600 m of altitude point to its stabilization at 2.4 ± 0.4 ka (Fig. 13C). It seems that the two sectors of the glacier front behave differently, unless the rock glacier front boulders still retain nuclide inheritance (Çiner et al., 2017), as suggested above. This debris-covered glacier

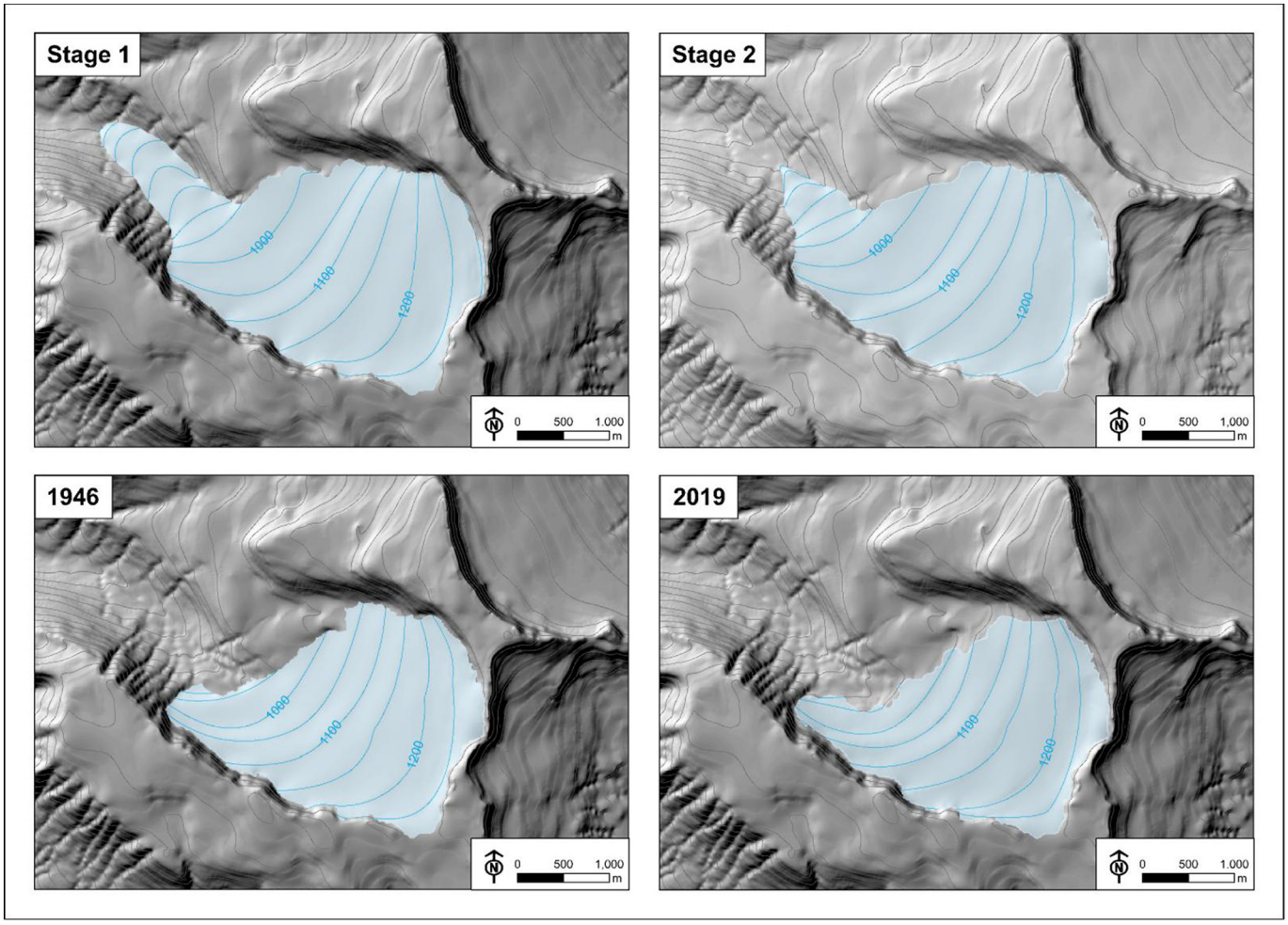

Fig. 11. Three-dimensional glacier reconstructions of the Héðinsdalsjökull glacier in the Stages 1 (Neoglacial maximum), 2 (LIA maximum), 1946 and 2019.

seems completely collapsed and most likely no longer preserves any underlying ice. Lichen coalescence observed in all lichenometric sampling points on the collapsed sector suggests that the complete degradation until 820 m occurred prior to 160–200 years ago (Maizels and Dugmore, 1985; Thompson and Jones, 1986; Evans et al., 1999).

(iv) *Advance of the (active) debris-covered glacier, subsidence and subsequent readvances.* Both the rock glacier and the collapsed debris-covered glacier are overlapped by frontal moraines that connect with the currently active debris-covered glacier (Fig. 13D). Geomorphological evidence shows that, after advancing and overlapping the preceding features, this glacier started to retreat through a slow subsidence, which still is in progress (Figs. 12D, 13D, 12E). This pattern is characteristic of shrinking debris-covered glaciers (Kirkbride, 2000, 2011; Brenning, 2005; Grindvik-Knudsen et al., 2006; Azócar and Brenning, 2010; Janke et al., 2013; Monnier and Kinnard, 2016). This subsidence process might have stopped, and even the glacier was able to advance at least twice or three times, as revealed by the number of push frontal moraines (Figs. 12E, 13E). According to the minimum ages indicated by the lichens, the maximum advance occurred prior to 160–200 years ago. Upslope, the next push moraine yields a lichen age corresponding to the beginning of the 19th century.

Table 6
Surface exposure ages estimated from Kugelmann's (1991) 0.44 mm yr^{-1} growth rate for *Rhizocarpon geographicum* (RG) and 0.737 mm yr^{-1} and *Porpidia soredizodes* (PS) lichen assuming growth rate and a 10, 15 and 20-year colonization lag, following Fernández-Fernández et al. (2019). The more probable colonization ages for *Rhizocarpon geographicum* is 20 years and for *Porpidia soredizodes* is 10 years (Fernández-Fernández et al., 2019) and these ages are outstanding in the table and in the text.

Lichen station (LS)	*Rhizocarpon geographicum* (*RG*) Min. circ. diameter (mm)	Porpidia soredizodes (PS) Min. circ. diameter (mm)	RG/PS Surface date from growth rate *10-yr col. lag*	RG/PS Surface date from growth rate *15-yr col. lag*	RG/PS Surface date from growth rate *20-yr col. lag*
1–2–3-4-5	Coalescing thalli	Coalescing thalli			
6	83.3	131.1	1811/1821	1806/1816	1801/1811
7	37.2	65.7	1914/1909	1909/1904	1904/1899
8	26.3	44.9	1939/1938	1934/1933	1929/1928
9	18.7	41.4	1956/1942	1951/1937	1946/1932
10	23.5	44.2	1945/1939	1940/1934	1935/1929
11	0	5.6	/1997	/1992	/1987

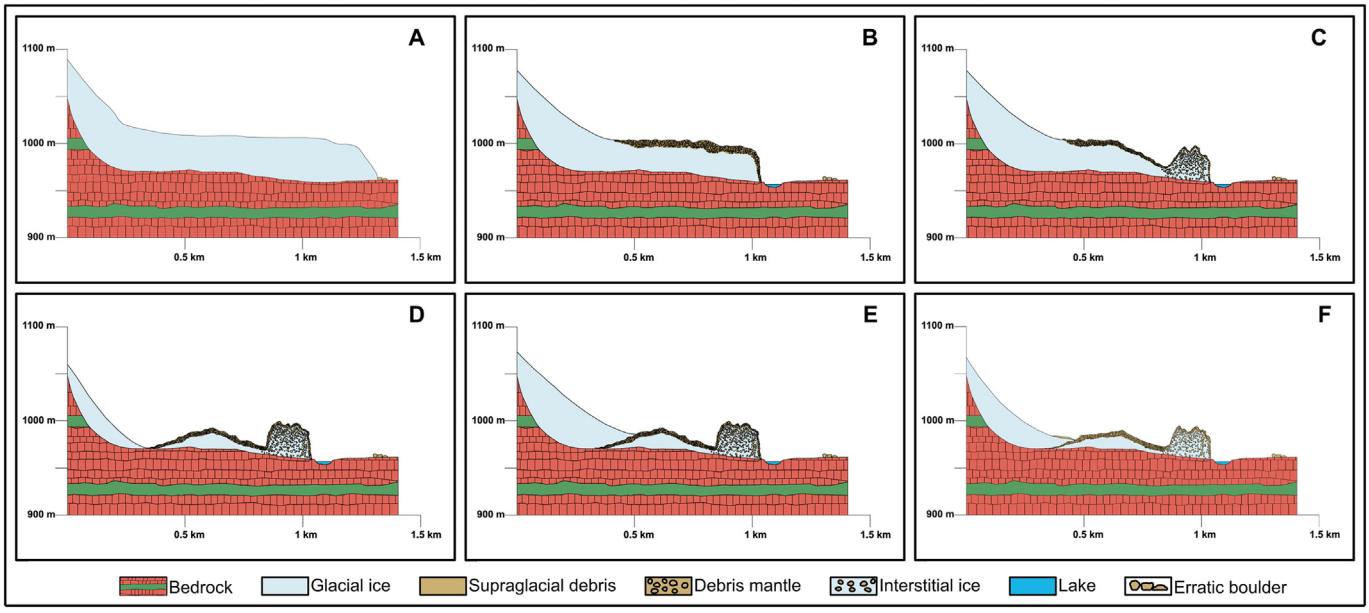

Fig. 12. Idealized model of the evolution of transect A-A', in the northern sector of the Héðinsdalsjökull glacier on the platform (960 m) according to the CRE ages. See location of this transect in the Fig. 3A. A) A debris-free glacier deposited the cirque around 8–7 ka. B) The glacier left a moraine at 8–6 ka, then started to retreat and the frontal-glacial depression was formed. C) Just after the onset of the retreat of the glacier rock, a glacier was formed and its front rapidly stabilized. CRE uncertainties does not allow establishing the exact chronology of the phases A, B and C. Subsequently, the roots of the rock glacier have been stabilizing slowly until the present day. D) The glacier readvanced and overlapped the rock glacier. Afterwards, the glacier, transformed in a debris-covered glacier, retreated and shrank due to ice melting and subsidence. An ice core is still present in this debris-covered sector of the glacier, behind the rock glacier. E) The glacier readvanced recently as a debris-free glacier and overlapped the debris-covered glacier. F) The debris-free glacier has undergone a strong retreat within the last decades.

However, this must be considered as an approximate age, since it is close to the maximum age limit of the lichenometry in Iceland and the decrease of the lichen growth rate after the "lineal" phase is operating, as it was verified in neighboring valleys (Fernández-Fernández et al., 2019). The only reference to the glacier termini position following this date is the innermost frontal moraine of the active debris-covered glacier, which was abandoned between 1899 and 1914 CE (Table 6).

(v) *A debris-free glacier advance and the formation of an incipient rock glacier*. The 1946 photo shows an ice-cored push moraine in the westernmost sector of the glacier front (see Fig. 13F). In 2000 and 2019, this sector includes a small rock glacier, already detached from the glacier front. Therefore, we interpret

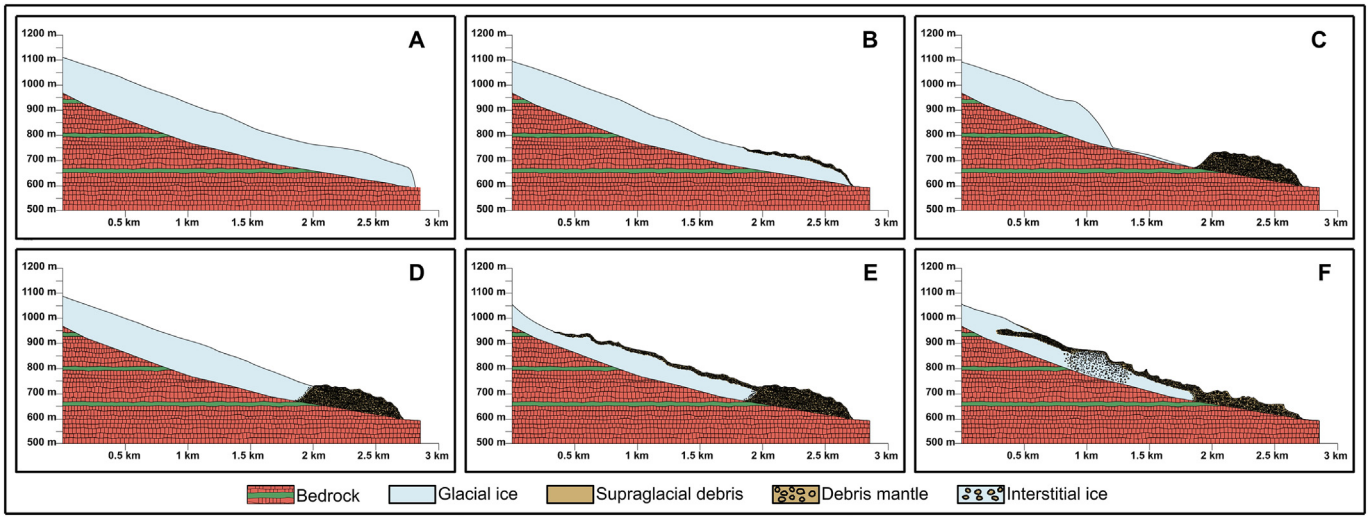

Fig. 13. Idealized model of the evolution of transect B-B′, in the southern sector of the Héðinsdalsjökull glacier embedded in the valley, according to the CRE and lichenometric dating. See location of this transect in the Fig. 3A. A) A debris-free glacier embedded in the valley is hypothesized, but all evidence has been subsequently removed by intense slope processes. B) A debris-covered glacier was formed due to very active paraglacial activity. C) The front of the debris-covered glacier collapsed around 3–2 ka. D) The debris-free glacier readvanced and overlapped the collapsed debris-covered glacier. A maximum advance of this glacier during the 15th and 17th centuries (LIA) is assumed. Afterwards, the glacier retreated again and its only dynamic is the surface subsidence due to the ice melting. There is still an ice core in the debris covered glacier behind the collapsed debris-covered glacier. E) Minor advances occurred at the onset of the 19th century as the latest, during the beginning of 20th century and between 1960 and 1990. Its last readvance occurred as a debris-free glacier, overlapping the active debris-covered glacier. The debris-free glacier has undergone a strong retreat within the last decades. A proto-rock glacier is derived from a pre-1946 ice-cored moraine.

it as the genesis of an ice-core moraine-derived rock glacier originated in the 1940s–1950s. The moderate slope gradient of the slope, where the moraine was located, favored the gravitationally-induced creep of the ice-cored moraine. Ages of lichens measured on this incipient rock glacier gave dates between 1939 and 1946, which are in good agreement with the abandonment of the moraine close to 1946. The slow subsidence processes allow lichens to survive in some boulders, as it was also observed in adjacent cirques (Fernández-Fernández et al., 2019).

(vi) *Further advance of the debris-free glacier and subsequent retreat*. The snout of the current debris-free glacier advanced and overlapped the active debris-covered glacier in many places. Later, its front retreated or, at least, thinned (Figs. 12F and 13F). This overlapping was observed in the fieldwork of 2018, especially in the terminus sector showing a thicker debris cover. This fact is confirmed by the contrast between the photos from 2000 and 2019: the glacier receded only where the front was debris-free. This is due to the absence of an isolating debris-cover protecting the underlying ice from the warming intensification initiated at the onset of the 21st century (Fernández-Fernández et al., 2017), which enhances the sensitivity of the glaciers to climate changes (e.g. Benn and Evans, 2010), a well-known issue in Northern Iceland (Caseldine, 1985; Häberle, 1991; Kugelmann, 1991; Fernández-Fernández et al., 2017, 2019). The *Porpidia soredizodes* lichens are present at the frontal moraine corresponding to the terminus position of the glacier shown in the aerial photo of 2000, and their size indicate a consistent date of 1997, considering 10-year colonization lag. However, there are no lichens of the *Rhizocarpon geographicum* species in this moraine, hindering us to verify the derived ages. Indeed, this result also supports the suitability of the application of 10-year colonization lag for the lichen species *Porpidia soredizodes* and the minimum 20-year colonization lag for the *Rhizocarpon geographicum* species (Fernández-Fernández et al., 2019).

6.2. The evolution of Héðinsdalsjökull in the context of the Tröllaskagi peninsula

The peculiarity of Héðinsdalsjökull relies on its complex glacial evolution. The multiple evolutionary stages follow a chronological sequence in good agreement with the results obtained in other valleys in Tröllaskagi. In the Fremri-Grjótárdalur and Hóladalur cirques, in the headwall of the Víðinesdalur valley (a parallel valley 12 km to the north), there are frontal moraines (at 830 m) very close to the current glaciers dated at 11.3 ± 0.7 and 10.6 ± 1.0 ka ($n = 2$), respectively (Fernández-Fernández et al., 2020). At this time, recent exposure dating of erratic boulders indicate that the IIS outlet glacier flowing down through Skagafjörður fjord had retreated almost to its current position in the highlands (Andrés et al., 2019). These glaciers could have evolved into rock glaciers (Fremri-Grjótárdalur cirque) and a debris-covered glacier (Hóladalur cirque). This was due to the intensification of paraglacial dynamics on the recently deglaciated cirque walls, once they remained ice-free and debutressed with the subsequent increase of debris supply (Ballantyne, 2002; Fernández-Fernández et al., 2020). In fact, the lower elevation fronts of Fremri-Grjótárdalur rock glaciers (at ~870 m) became inactive at 10.8 ± 0.7 ka (n = 2) and the higher ones (~1020 m) at 9.3 ± 0.7 ka (n = 2) (Fernández-Fernández et al., 2020), in coincidence with the maximum retreat of all the Icelandic glaciers (Larsen et al., 2012; Geirsdóttir et al., 2019). In summary, with the beginning of the Holocene, the debris-free glaciers distributed in these cirques receded due to widespread warming in high latitudes and formed rock glaciers, whose fronts stabilized and became relict shortly after.

Similar pattern to that in Fremri-Grjótárdalur and Hóladalur cirques occurred in the Héðinsdalsjökull glacier front, located on the upper plateau at 930 m. In this case, the debris-free glacier receded later, at 6.7 ± 0.9 ka. These CRE ages indicate that the retreat of the glacier overlaps with the end of the HTM (Kirkbride and Dugmore, 2006). Behind this moraine deposited by a debris-free glacier, a rock glacier with an internal ice core exists. Studies in the nearby abovementioned rock glaciers show that, despite the ice cores, the movement of these landforms located in gentle slopes is very slow and fundamentally related to ice melting and subsidence (Andrés et al., 2016; Tanarro et al., 2019; Campos et al., 2019). These circumstances allow the boulders to remain stable on the surface of the rock glacier or debris-covered glacier for about 4 to 7 ka, which allows obtaining CRE dating indicative of flow stagnation from them (Fernández-Fernández et al., 2020). Results obtained in the Fremri-Grjótárdalur rock glacier and in the Hóladalur debris-covered glacier gave mean ages of 4.7 ± 0.5 ka ($n = 3$) and 5.8 ± 0.7 ka (n = 3), respectively (Fernández-Fernández et al., 2020). These Mid-Holocene ages are close to our results in the front of the rock glacier of Héðinsdalsjökull of 6.3 ± 0.9 ka, which in turn is very similar to that of the moraine located in front of the rock glacier. This seems to confirm that the retreat of a debris-free glacier was followed by its rapid transformation into a rock glacier, whose front stagnated at the end of the HTM despite still preserving an ice core.

Information on the previous glacial evolution at the bottom of the valley during much of the Holocene is limited. We only have data on the stabilization of the debris-covered glacier, from its front at ~600 m to 820 m at 2.4 ± 0.4 ka (n = 3). This age coincides with some of the Neoglacial advances detected in Iceland (Stötter et al., 1999; Kirkbride and Dugmore, 2006, 2008) and with an important cold period (Andersen et al., 2004; Geirsdóttir et al., 2009, 2013, 2019). The Tungnahryggsjökull debris-free glaciers, located 7 km N of Héðinsdalsjökull, reveal Neoglacial glacial culminations at 1.6 and 1.3 ka (Dark Ages Cold Period) (Fernández-Fernández et al., 2019), although these glaciers might have experienced other earlier Neoglacial advances. The ELAs of the maximum advance of the debris-covered glacier (Stage 1) in Héðinsdalsjökull (1042–1062 m) and the dated Neoglacial advances of the debris-free glaciers of Vesturdalur and Austuradalur (~1030-~1050 m; Fernández-Fernández et al., 2019) report very similar values. However, CRE results suggest that the Héðinsdalsjökull glacier limits in Stage 1 do not exactly correspond to a single phase, but they encompass glacial oscillations corresponding to a period between 7 and 2 ka.

The lower collapsed debris-covered glacier is overlapped by a frontal moraine from the active debris-covered glacier. The age of this moraine is unknown. This advance might have occurred during the LIA, the greatest cooling of the second half of the Holocene in Iceland (Larsen et al., 2012). The ELA of this maximum advance of the active debris-covered Héðinsdalsjökull is similar to the maximum advance of the Tungnahryggsjökull glaciers in Vesturdalur and Austurdalur during the 15th and 17th centuries, i.e. the LIA (1050–1060 m; Fernández-Fernández et al., 2019). The two internal frontal moraines of the active debris-covered glacier were abandoned by the glacier between 1811 and 1821, and between 1904 and 1919 CE. Moraines of similar ages have been identified in the forelands of the two debris-free glaciers of Vesturdalur and Austurdalur (Fernández-Fernández et al., 2019). The evolution of the ELA in Héðinsdalsjökull between 1946 and 2000 shows a rise from 1085 to 1095 m. These values are close to those observed in the Western Tungnahryggsjökull (1094 and 1098 m) in the same dates (Fernández-Fernández et al., 2019). The evolution of the ELA of the Héðinsdalsjökull is very similar to that of Western Tungnahryggsjökull. Thus, during other previous undated periods, such as the LIA, the ELAs between both glaciers might have also been consistent. Consequently, the moraine deposits of the present debris-free glacier, that overlapped the active debris-covered glacier, might be contemporaneous with the glacial advance detected in Tungnahryggsjökull glaciers, and in other glaciers of the peninsula from the mid-1970s to the mid-1990s (Fernández-Fernández et al., 2017, 2019).

The dynamic behaviour of the debris-covered and the rock glacier in the Héðinsdalur cirque is related to the permafrost layer in Tröllaskagi. The lower section of the debris-covered glacier lost the ice core and collapsed just below the current lower limit of permafrost at 800–900 m (Czekirda et al., 2019; Etzelmüller et al., 2007, 2020). Therefore, at higher elevations, the active rock glacier (900 m) and the debris-covered glacier (850 m) still preserve the ice core although with a tendency to slow subsidence, as occurs in other cirques of the peninsula (Tanarro et al., 2019; Campos et al., 2019). This current ice subsidence must correspond to the gradual rise in the level of permafrost in Northern Iceland since the end of the LIA (Etzelmüller et al., 2020).

The abundance of debris-covered glaciers and rock glaciers in Tröllaskagi cirques is undoubtedly in direct relation to the slope active processes in these mountains (Jónsson, 1976; Whalley et al., 1983; Mercier et al., 2013; Cossart et al., 2014; Decaulne et al., 2016; Sæmundsson et al., 2018). The few currently debris-free glaciers such as Héðinsdalsjökull and Tungnahryggsjökull (especially the eastern one) are located precisely in those cirques whose headwalls are to a great part covered by ice, while the debris-covered glaciers and rock glaciers are systematically found in the cirques where the headwalls are mostly ice-free well standing out above the glacier surface (Fernández-Fernández et al., 2019, 2020).

6.3. The complex evolution of Héðinsdalsjökull as result of an intricate coupling of paraglacial processes to climatic variability inside glacial cirques

Knowledge about the factors driving the genesis and evolution of debris-covered glaciers is of increasing importance, because its transformation from debris-free glaciers is being observed worldwide as an indicator of climate change. Nowadays, 7.3% of the mountain glacier area correspond to debris-covered glaciers, and more than 20% of these have debris-covered sectors (Herreid and Pellicciotti, 2020). The number and extent of debris-covered glaciers, as well as the debris-covered sectors of mostly debris-free glaciers, have significantly increased over the last decades as a consequence of rising temperatures, as it has been clearly detected in the Alps (Deline, 2005; Kellerer-Pirklbauer et al., 2008), Caucasus (Lambrecht et al., 2011; Tielidze et al., 2020), Himalaya (Shukla et al., 2009; Bhambri et al., 2011; Thakuri et al., 2014; Scherler and Egholm, 2020), Patagonia (Glasser et al., 2016), and in the Southern Alps of New Zealand (Quincey and Glasser, 2009). Understanding mass balance, surface flow and spatio-temporal dynamics of these debris-covered glaciers is of great importance for a better prediction of global sea-level rise (Herreid and Pellicciotti, 2020) as well as for managing increasing cryospheric hazards (Ding et al., 2021). In this context, the evolution of Héðinsdalsjökull described in this work opens new perspectives, as it shows a much more complex scenario than the generally accepted theory, proposing the straight transformation of debris-free into debris-covered glaciers and rock glaciers as part of a gradual and staggered process (Berthling, 2011; Monnier and Kinnard, 2015, 2016; Janke et al., 2013, 2015; Anderson et al., 2018a; Hambrey et al., 2008; Rowan et al., 2015; Jones et al., 2019; Knight et al., 2019). Here, we demonstrate that the same debris-free glacier can retreat and evolve into a rock glacier in some sectors whereas in others it can generate a debris-covered glacier. Subsequently, the debris-covered glacier and rock glacier can evolve into a debris-free glacier when favorable climatic conditions trigger a glacial advance. Then, the advancing ice can overlap static and disconnected ice-cored formations distributed in front of it. This has occurred in Héðinsdalur cirque at least twice, namely during the LIA maximum and since the mid-1970s to mid-1990s, the last advances of the 20th century.

The great sensitivity of Icelandic debris-free glaciers to climatic fluctuations (Caseldine, 1985; Häberle, 1991; Kugelmann, 1991; Fernández-Fernández et al., 2017, 2019) and the typically delayed response of debris-covered and rock glaciers to climate changes (Andrés et al., 2016; Tanarro et al., 2019; Campos et al., 2019) can be detected in the terminal area of the Héðinsdalsjökull glacier. On the one hand, the glacier readjusts to the new paraglacial conditions, which in the case of Tröllaskagi peninsula are enhanced by the weakness of the walls (Whalley et al., 1983), as well as by fast deglaciation (Andrés et al., 2019). As observed in other mountain and polar regions, both factors are crucial to enhance paraglacial processes in recently deglaciated environments (Spreafico et al., 2021). Paraglacial processes provoke surge-like short term advances of the glacier front, with no connection to climatic variability, even in low-angle mountain glaciers (Kääb et al., 2021). These glacial advances, resulting from massive supply from the readjusting slopes during the paraglacial phase, are usually followed by ice stagnation and slow deposition of hummocky moraines, which generate a landscape very different to moraine ridges built during phases of favorable paleoclimatic conditions (Vacco et al., 2010).

On the other hand, in Héðinsdalsjökull, a debris-free glacier advances from the head and recedes in pace with the short-term climatic fluctuations, whereas the active debris-covered glacier and the rock glacier are currently subjected to a slow subsidence process. The existence of debris-free ice sections in the headland of the rock glaciers has been cited since the first definition of this landform (Capps, 1910), although it has been always considered as a part connected to the rock glacier and, indeed, from where it receives its feeding of ice (e.g. Giardino and Vitek, 1988; Whalley and Martin, 1992; Whalley et al., 1995; Barsch, 1996; Potter et al., 1998; Janke et al., 2013). A similar process has been described also in debris-covered glaciers (e.g. Kirkbride, 2011). Moreover, it is worth noting that until now, the independent and autonomous response to climate shifts of this debris-free ice section in the headlands of the rock glaciers and debris covered glaciers has not been described.

An additional complication arises from the fact that rock glaciers and debris-covered glaciers can reflect slope processes not directly linked with climate (Kirkbride, 2000; Brenning, 2005; Azócar and Brenning, 2010; Deline et al., 2015; Anderson and Anderson, 2016; Mayr and Hagg, 2019). Debris-covered glaciers descending from ice sheets or large ice caps are an exception, and can show a high sensitivity to climate changes (Charton et al., 2020). Moreover, climate warming can directly influence the dynamic pattern of both formations, reducing their flow and even stagnating them, mainly when they are low-angle as in Tröllaskagi, with the subsequent stabilization of their deposits and frequent formation of thermokarst features (Potter et al., 1998; Janke et al., 2013; Emmer et al., 2015; Anderson et al., 2018a; Tanarro et al., 2019; Storni et al., 2020; Ferguson and Vieli, 2020). This may explain that the Héðinsdalsjökull rock glacier front has remained stable since its formation during the HTM until the present, still preserving its ice core. This stabilization can be chronologically constrained by CRE ages (Hippolyte et al., 2009; Deline et al., 2015; Moran et al., 2016; Fernández-Fernández et al., 2017; Crump et al., 2017; Palacios et al., 2016, 2017, 2020; Andrés et al., 2018; Dede et al., 2017; Winkler and Lambiel, 2018; Charton et al., 2020; Linge et al., 2020; Steinemann et al., 2020; Amschwand et al., 2021; Jomelli et al., 2020), suggesting that these formations can remain stable even if they still have an inner ice core (Mackay and Marchant, 2016; Fernández-Fernández et al., 2020; Amschwand et al., 2021; Scherler and Egholm, 2020). Moreover, a large number of CRE samples is necessary to reach solid conclusions on the age of this stabilization (Moran et al., 2016; Crump et al., 2017; Charton et al., 2020).

The short time elapsed since the formation of the debris-free-glacier moraine and the formation of the rock glacier in Héðinsdalsjökull is driven by the very intense paraglacial processes, as it has been also observed in other areas, such as in Northern Iceland (Fernández-Fernández et al., 2020), the Alps (Hippolyte et al., 2009; Moran et al., 2016; Le Roy et al., 2017; Steinemann et al., 2020; Amschwand et al., 2021), Mediterranean mountains (Fernández-Fernández et al., 2017; Dede et al., 2017; Palacios et al., 2016, 2017, 2020; Andrés et al., 2018; Jomelli et al., 2020) and the Southern Alps (Winkler and Lambiel, 2018). In fact, a rock glacier can form even within only a hundred years following the onset of deglaciation (Linge et al., 2020). This fact may explain the beginning of the formation of a proto-rock glacier derived from a push moraine only a few decades ago. Although the rock

glacier front of Héðinsdalsjökull has remained stable for thousands of years, its sector close to the valley head can subsequently stabilize much later, as it has been shown in the Mediterranean mountains (Palacios et al., 2016, 2017, 2020; Jomelli et al., 2020) and the Alps (Hippolyte et al., 2009; Moran et al., 2016; Steinemann et al., 2020; Amschwand et al., 2021).

In summary, the evolution of Héðinsdalsjökull complex results from a rapid response to paraglacial processes and a slow reaction to climate changes. The rapid paraglacial readjustment has been previously demonstrated in other mountains (Deline et al., 2015; Anderson and Anderson, 2016; Mayr and Hagg, 2019). In this work, we have shown that the formation of rock glaciers and debris-covered glaciers can be reversed: the debris-covered glacier evolved into a debris-free glacier, with great sensitivity to climate change. Indeed, this new debris-free glacier left moraines of similar age than those generated by others debris-free glaciers in the same region, similar to what happened during the LIA and over the last decades.

7. Conclusions

Héðinsdalsjökull evolution is particularly complex. From the existence of a debris-free glacier, its retreat during the HTM led to rapid transformation into a variety of glacier states, conditioned by the intensification of paraglacial processes. While the front at the lower sector (600 m), embedded in the bottom of the valley, transformed into a debris-covered glacier, the margin located on a platform at 900 m evolved into a rock glacier. The front of this rock glacier stabilized shortly after it formed, around 7–6 ka, although its roots remained active much longer. The lowest part of the debris-covered glacier (between 600 and 820 m) stabilized about 2.4 ka ago. Since then, geomorphological evidence shows that Héðinsdalsjökull has undergone several phases of advance and retreat. It probably reached its maximum advance during the LIA, in the 15th to 17th centuries, as it happened in neighboring glaciers, with new re-advances at the beginning of the 19th and 20th centuries. After a significant retreat, the glacier advanced around 1990s, and then retreated again, in accordance with the regional climatic evolution. The ice-core of the debris-covered glaciers and rock glaciers survive until the present, thanks to their location above the local lower limit of the permafrost, although they are slowly degrading through a process of subsidence. In parallel, a proto-rock glacier originated from an ice-cored moraine since around 1940–1950 CE. The influence of paraglacial processes on the formation of a debris-covered glacier and rock glacier and their subsequent slow evolution is consistent with the pattern already observed in other mountains. What is exceptional is that both dynamics occur synchronously in the same glacier and that, contrary to the generally accepted evolutionary models, a glacier composed of a debris-covered glacier and rock glacier can later transform into a debris-free glacier, with high sensitivity to climatic fluctuations.

Declaration of competing interest

The authors declare that they have no known competing financial interests or personal relationships that could have appeared to influence the work reported in this paper.

Acknowledgements

This paper was funded by PR108/20-20 (Santander Bank-UCM Projects) and Nils Mobility Program (EEA GRANTS), and with the help of the High Mountain Physical Geography Research Group (Universidad Complutense de Madrid). We thank the Icelandic Association for Search and Rescue, the Icelandic Institute of Natural History, the Hólar University College, David Palacios Jr. and María Palacios for their support in the field. José M. Fernández-Fernández is supported by a postdoctoral grant within the NUNANTAR project (02/SAICT/2017 32002; Fundação para a Ciência e a Tecnologia, Portugal). Marc Oliva is supported by the Ramón y Cajal Program (RYC-2015-17597) and by the Research Group ANTALP (Antarctic, Arctic, Alpine Environments; 2017-SGR-1102) funded by the Government of Catalonia. The ^{36}Cl measurements were performed at the ASTER AMS national facility (CEREGE, Aix en Provence), which is supported by the INSU/CNRS and the ANR through the "Projets thématiques d'excellence" program for the "Equipements d'excellence" ASTER-CEREGE action and IRD. The authors are grateful for the comments and suggestions of Dr. Jasper Knight and anonymous reviewer, which have considerably improved the quality of the manuscript.

Appendix A. Supplementary data

Supplementary data associated with this article can be found in the online version, at https://doi.org/10.1016/j.geomorph.2021.107787. These data include the Google map of the most important areas described in this article.

References

Amschwand, D., Ivy-Ochs, S., Frehner, M., Steinemann, O., Christl, M., Vockenhuber, C., 2021. Deciphering the evolution of the Bleis Marscha rock glacier (Val d'Err, eastern Switzerland) with cosmogenic nuclide exposure dating, aerial image correlation, and finite-element modelling. Cryosphere Discuss. 15, 2057–2081. https://doi.org/10.5194/tc-2020-209.

Andersen, C., Koç, N., Moros, M., 2004. A highly unstable Holocene climate in the subpolar North Atlantic: evidence from diatoms. Quat. Sci. Rev. 23, 2155–2166. https://doi.org/10.1016/j.quascirev.2004.08.004.

Anderson, L.S., Anderson, R.S., 2016. Modeling debris-covered glaciers: response to steady debris deposition. Cryosphere. 10, 1105–1124. https://doi.org/10.5194/tc-10-1105-2016.

Anderson, R.S., Anderson, L.S., Armstrong, W.H., Rossi, M.W., Crump, S.E., 2018a. Glaciation of alpine valleys: the glacier–debris-covered glacier–rock glacier continuum. Geomorphology 311, 127–142. https://doi.org/10.1016/j.geomorph.2018.03.015.

Anderson, L.S., Flowers, G.E., Jarosch, A.H., Aðalgeirsdóttir, G.T., Geirsdóttir, Á., Miller, G.H., Harning, D.J., Thorsteinsson, T., Magnússon, E., Pálsson, F., 2018b. Holocene glacier and climate variations in Vestfirðir, Iceland, from the modeling of Drangajökull ice cap. Quat. Sci. Rev. 190, 39–56. https://doi.org/10.1016/j.quascirev.2018.04.024.

Andrés, N., Tanarro, L.M., Fernández, J.M., Palacios, D., 2016. The origin of glacial alpine landscape in Tröllaskagi Peninsula (North Iceland). Cuad. Investig. Geográfica 42, 341–368. https://doi.org/10.18172/cig.2935.

Andrés, N., Gómez-Ortiz, A., Fernández-Fernández, J.M., Tanarro, L.M., Salvador-Franch, F., Oliva, M., Palacios, D., 2018. Timing of deglaciation and rock glacier origin in the southeastern Pyrenees: a review and new data. Boreas 47, 1050–1071. https://doi.org/10.1111/bor.12324.

Andrés, N., Palacios, D., Sæmundsson, Þ., Brynjólfsson, S., Fernández-Fernández, J.M., 2019. The rapid deglaciation of the Skagafjörður, northern Iceland. Boreas 48 (1), 92–106. https://doi.org/10.1111/bor.12341.

Azócar, G., Brenning, A., 2010. Hydrological and geomorphological significance of rock glaciers in the dry Andes, Chile (27°-33°S). Permafr. Periglac. Process. 21 (1), 42–53. https://doi.org/10.1002/ppp.669.

Ballantyne, C.K., 2002. Paraglacial geomorphology. Quat. Sci. Rev. 21, 1935–2017. https://doi.org/10.1016/S0277-3791(02)00005-7.

Ballantyne, C.K., 2013. Paraglacial geomorphology. Encyclopedia of Quaternary Science, Second edition Elsevier, pp. 553–565 https://doi.org/10.1016/B978-0-444-53643-3.00089-3.

Barr, I.D., Spagnolo, M., 2015. Glacial cirques as palaeoenvironmental indicators: their potential and limitations. Earth Sci. Rev. 151, 48–78. https://doi.org/10.1016/j.earscirev.2015.10.004.

Barr, I.D., Ely, J.C., Spagnolo, M., Clark, C.D., Evans, I.S., Pellicer, X.M., ... Rea, B.R., 2017. Climate patterns during former periods of mountain glaciation in Britain and Ireland: Inferences from the cirque record. Palaeogeogr. Palaeoclimatol. Palaeoecol. 485, 466–475. https://doi.org/10.1016/j.palaeo.2017.07.001.

Barsch, D., 1996. Rock Glaciers. Springer, Berlin 331 pp.

Barth, A.M., Clark, P.U., Clark, J., McCabe, A.M., Caffee, M., 2016. Last Glacial Maximum cirque glaciation in Ireland and implications for reconstructions of the Irish Ice Sheet. Quat. Sci. Rev. 141, 85–93. https://doi.org/10.1016/j.quascirev.2016.04.006.

Benedict, J.B., 1973. Chronology of cirque glaciation, Colorado front range. Quat. Res. 3 (4), 584–599. https://doi.org/10.1016/0033-5894(73)90032-X.

Beniston, M., Farinotti, D., Stoffel, M., Andreassen, L.M., Coppola, E., Eckert, N., Fantini, A., Giacona, F., Hauck, C., Huss, M., Huwald, H., Lehning, M., López-Moreno, J.I., Magnusson, J., Marty, C., Moran-Tejéda, E., Morin, S., Naaim, M., Provenzale, A., Rabatel, A., Six, D., Stötter, J., Strasser, U., Terzago, S., Vincent, C., 2018. The European mountain cryosphere: a review of its current state, trends, and future challenges. Cryosphere 12 (2), 759–794. https://doi.org/10.5194/tc-12-759-2018.

Benn, D.I., Evans, D.J.A., 2010. Glaciers and Glaciation. 2nd edition. Arnold, London 734 p.

Benn, D.I., Hulton, N.R.J., 2010. An ExcelTM spreadsheet program for reconstructing the surface profile of former mountain glaciers and ice caps. Comput. Geosci. 36, 605–610. https://doi.org/10.1016/j.cageo.2009.09.016.

Berthling, I., 2011. Beyond confusion: rock glaciers as cryo-conditioned landforms. Geomorphology 131, 98–106. https://doi.org/10.1016/j.geomorph.2011.05.002.

Bhambri, R., Bolch, T., Chaujar, R.K., Kulshreshtha, S.C., 2011. Glacier changes in the Garhwal Himalaya, India, from 1968 to 2006 based on remote sensing. J. Glaciol. 57, 543–556. https://doi.org/10.3189/002214311796905604.

Bradwell, T., 2001. A new lichenometric dating curve for southeast Iceland. Geogr. Ann. A Phys. Geogr. 83 (3), 91–101. https://doi.org/10.1111/j.0435-3676.2001.00146.x.

Braucher, R., Keddadouche, K., Aumaître, G., Bourlès, D.L., Arnold, M., Pivot, S., ... Bard, E., 2018. Chlorine measurements at the 5MV French AMS national facility ASTER: Associated external uncertainties and comparability with the 6MV DREAMS facility. Nucl. Instrum. Methods Phys. Res., Sect. B 420, 40–45. https://doi.org/10.1016/j.nimb.2018.01.025.

Brenning, A., 2005. Geomorphological, hydrological and climatic significance of rock glaciers in the Andes of Central Chile (33-35°S). Permafr. Periglac. Process. 16, 231–240. https://doi.org/10.1002/ppp.528.

Campos, N., Tanarro, L.M., Palacios, D., Zamorano, J.J., 2019. Slow dynamics in debris-covered and rock glaciers in Hofsdalur, Tröllaskagi Peninsula (northern Iceland). Geomorphology. 342, 61–77. https://doi.org/10.1016/j.geomorph.2019.06.005.

Capps Jr., S.R., 1910. Rock glaciers in Alaska. J. Geol. 18 (4), 359–375. https://doi.org/10.1086/621746.

Caseldine, C., 1983. Resurvey of the margins of Gljúfurárjökull and the chronology of recent deglaciation. Jökull 33, 111–118.

Caseldine, C.J., 1985. The Extent of some Glaciers in Northern Iceland during the Little Ice Age and the Nature of recent Deglaciation. Geogr. J. 151, 215–227. https://doi.org/10.2307/633535.

Caseldine, C.J., Cullingford, R.A., 1981. Recent mapping of Gljúfurárjökull and Gljúfurárdalur. Jökull 31, 11–22.

Caseldine, C.J., Stotter, J., 1993. "Little Ice Age" glaciation of Tröllaskagi peninsula, northern Iceland: Climatic implications for reconstructed equilibrium line altitudes (ELAs). The Holocene 3, 357–366. https://doi.org/10.1177/095968369300300408.

Charton, J., Jomelli, V., Schimmelpfennig, I., Verfaillie, D., Favier, V., Mokadem, F., ... Keddadouche, K., 2020. A debris-covered glacier at Kerguelen (49° S, 69° E) over the past 15 000 years. Antarct. Sci. 33, 1–13. https://doi.org/10.1017/S0954102020000541.

Chenet, M., Roussel, E., Jomelli, V., Grancher, D., 2010. Asynchronous Little Ice Age glacial maximum extent in southeast Iceland. Geomorphology 114, 253–260. https://doi.org/10.1016/j.geomorph.2009.07.012.

Çiner, A., Sarıkaya, M.A., Yıldırım, C., 2017. Misleading old age on a young landform? The dilemma of cosmogenic inheritance in surface exposure dating: moraines vs. rock glaciers. Quat. Geochronol. 42, 76–88. https://doi.org/10.1016/j.quageo.2017.07.003.

Cossart, E., Mercier, D., Decaulne, A., Feuillet, T., Jónsson, H.P., Saemundsson, Þ., 2014. Impacts of post-glacial rebound on landslide spatial distribution at a regional scale in northern Iceland (Skagafjörður). Earth Surf. Process. Landf. 39, 336–350. https://doi.org/10.1002/esp.3450.

Crochet, P., Jóhannesson, T., Jónsson, T., Sigurðsson, O., Björnsson, H., Pálsson, F., Barstad, I., 2007. Estimating the spatial distribution of precipitation in Iceland using a linear model of orographic precipitation. J. Hydrometeorol. 8, 1285–1306. https://doi.org/10.1175/2007JHM795.1.

Crump, S.E., Anderson, L.S., Miller, G.H., Anderson, R.S., 2017. Interpreting exposure ages from ice-cored moraines: a Neoglacial case study on Baffin Island, Arctic Canada. J. Quat. Sci. 32 (8), 1049–1062. https://doi.org/10.1002/jqs.2979.

Czekirda, J., Westermann, S., Etzelmüller, B., Jóhannesson, T., 2019. Transient modelling of permafrost distribution in Iceland. Front. Earth Sci. 7, 130. https://doi.org/10.3389/feart.2019.00130.

Dahl, S.O., Nesje, A., 1992. Palaeoclimatic implications based on equilibrium-line altitude depressions of reconstructed Younger Dryas and Holocene cirque glaciers in inner Nordfjord, western Norway. Palaeogeogr. Palaeoclimatol. Palaeoecol. 94 (1–4), 87–97. https://doi.org/10.1016/0031-0182(92)90114-K.

Decaulne, A., Cossart, E., Mercier, D., Feuillet, T., Coquin, J., Jónsson, H.P., 2016. An early Holocene age for the Vatn landslide (Skagafjörður, central northern Iceland): insights into the role of postglacial landsliding on slope development. The Holocene 26, 1304–1318. https://doi.org/10.1177/0959683616638432.

Dede, V., Çiçek, İ., Sarıkaya, M.A., Çiner, A., Uncu, L., 2017. First cosmogenic geochronology from the Lesser Caucasus: Late Pleistocene glaciation and rock glacier development in the Karçal Valley, NE Turkey. Quat. Sci. Rev. 164, 54–67. https://doi.org/10.1016/j.quascirev.2017.03.025.

Deline, P., 2005. Change in surface debris cover on Mont Blanc massif glaciers after the 'Little Ice Age' termination. Holocene 15, 302–309. https://doi.org/10.1191/0959683605hl809rrln.

Deline, P., Akçar, N., Ivy-Ochs, S., Kubik, P.W., 2015. Repeated Holocene rock avalanches onto the Brenva Glacier, Mont Blanc massif, Italy: a chronology. Quat. Sci. Rev. 126, 186–200. https://doi.org/10.1016/j.quascirev.2015.09.004.

Ding, Y., Mu, C., Wu, T., Hu, G., Zou, D., Wang, D., Wu, X., 2021. Increasing cryospheric hazards in a warming climate. Earth Sci. Rev. 103500. https://doi.org/10.1016/j.earscirev.2020.103500.

Dunne, J., Elmore, D., Muzikar, P., 1999. Scaling factors for the rates of production of cosmogenic nuclides for geometric shielding and attenuation at depth on sloped surfaces. Geomorphology 27, 3–11. https://doi.org/10.1016/S0169-555X(98)00086-5.

Dusik, J.M., Leopold, M., Heckmann, T., Haas, F., Hilger, L., Morche, D., Neugirg, F., Becht, M., 2015. Influence of glacier advance on the development of the multipart Riffeltal rock glacier, Central Austrian Alps. Earth Surf. Process. Landf. 40, 965–980. https://doi.org/10.1002/esp.3695.

Emmer, A., Loarte, E.C., Klimes, J., Vilímek, V., 2015. Recent evolution and degradation of the bent Jatunraju glacier (Cordillera Blanca, Peru). Geomorphology 228, 345–355. https://doi.org/10.1016/j.geomorph.2014.09.018.

Etzelmüller, B., Farbrot, H., Guðmundsson, Á., Humlum, O., Tveito, O.E., Björnsson, H., 2007. The regional distribution of mountain permafrost in Iceland. Permafr. Periglac. Process. 18, 185–199. https://doi.org/10.1002/ppp.583.

Etzelmüller, B., Patton, H., Schomacker, A., Czekirda, J., Girod, L., Hubbard, A., Lilleøren, K. S., Westermann, S., 2020. Icelandic permafrost dynamics since the Last Glacial Maximum - model results and geomorphological implications. Quat. Sci. Rev. 233, 106236. https://doi.org/10.1016/j.quascirev.2020.106236.

Evans, I.S., Cox, N.J., 1974. Geomorphometry and the operational definition of cirques. Area 6, 150–153.

Evans, I.S., Cox, N.J., 1995. The form of glacial cirques in the English Lake District, Cumbria. Z. Geomorphol. 39, 175–202. https://doi.org/10.1016/S0277-3791(98)00098-5.

Evans, D.J.A., Archer, S., Wilson, D.J.H., 1999. A comparison of the lichenometric and Schmidt hammer dating techniques based on data from the proglacial areas of some Icelandic glaciers. Quat. Sci. Rev. 18 (1), 13–41.

Evans, D.J., Ewertowski, M., Orton, C., 2017. Skaftafellsjökull, Iceland: glacial geomorphology recording glacier recession since the Little Ice Age. J. Maps 13 (2), 358–368. https://doi.org/10.1080/17445647.2017.1310676.

Farbrot, H., Etzelmuller, B., Guðmundsson, A., Humlum, O., Kellerer-Pirklbauer, A., Eiken, T., Wangensteen, B., 2007. Rock glaciers and permafrost in Trollaskagi, northern Iceland. Z. Geomorphol. 51, 1–16. https://doi.org/10.1127/0372-8854/2007/0051S2-0001.

Ferguson, J., Vieli, A., 2020. Modelling steady states and the transient response of debris-covered glaciers. Cryosphere Discuss., 1–31 https://doi.org/10.5194/tc-2020-228 (preprint).

Fernández-Fernández, J.M., Andrés, N., 2018. Methodological proposal for the analysis of the evolution of glaciers since the little ice age and its application in the Tröllaskagi Peninsula (Northern Iceland). Cuad. Investig. Geográfica Geogr. Res. Lett. 44, 69–97. https://doi.org/10.18172/cig.3392.

Fernández-Fernández, J.M., Andrés, N., Sæmundsson, Þ., Brynjólfsson, S., Palacios, D., 2017. High sensitivity of North Iceland (Tröllaskagi) debris-free glaciers to climatic change from the "Little Ice Age" to the present. The Holocene 27, 1–14. https://doi.org/10.1177/0959683616683262.

Fernández-Fernández, J.M., Palacios, D., Andrés, N., Schimmelpfennig, I., Brynjólfsson, S., Sancho, L.G., Zamorano, J.J., Heiðmarsson, S., Sæmundsson, Þ., 2019. A multi-proxy approach to Late Holocene fluctuations of Tungnahryggsjökull glaciers in the Tröllaskagi peninsula (northern Iceland). Sci. Total Environ. 664, 499–517. https://doi.org/10.1016/j.scitotenv.2019.01.364.

Fernández-Fernández, J.M., Palacios, D., Andrés, N., Schimmelpfennig, I., Tanarro, L.M., Brynjólfsson, S., López-Acevedo, F.J., Sæmundsson, Þ., Team, A.S.T.E.R., 2020. Constrains on the timing of debris-covered and rock glaciers: an exploratory case study in the Hólar área, nothern Iceland. Geomorphology 361, 107196. https://doi.org/10.1016/j.geomorph.2020.107196.

Fink, D., Vogt, S., Hotchkis, M., 2000. Cross-sections for 36Cl from Ti at Ep=35–150 MeV: applications to in-situ exposure dating. Nucl. Instruments Methods Phys. Res. Sect. B Beam Interact. Mater. Atoms 172, 861–866. https://doi.org/10.1016/S0168-583X(00)00200-7.

Geirsdóttir, Á., Miller, G.H., Axford, Y., Ólafsdóttir, Sædís, 2009. Holocene and latest Pleistocene climate and glacier fluctuations in Iceland. Quat. Sci. Rev. 28, 2107–2118. https://doi.org/10.1016/j.quascirev.2009.03.013.

Geirsdóttir, Á., Miller, G.H., Larsen, D.J., Ólafsdóttir, S., 2013. Abrupt Holocene climate transitions in the northern North Atlantic region recorded by synchronized lacustrine records in Iceland. Quat. Sci. Rev. 70, 48–62. https://doi.org/10.1016/j.quascirev.2013.03.010.

Geirsdóttir, Á., Miller, G.H., Andrews, J.T., Harning, D.J., Anderson, L.S., Florian, C., Larseb, D., Thordarson, T., 2019. The onset of Neoglaciation in Iceland and the 4.2 ka event. Clim. Past 15, 25–40. https://doi.org/10.5194/cp-15-25-2019.

Giardino, J.R., Vitek, J.D., 1988. The significance of rock glaciers in the glacial periglacial landscape continuum. J. Quat. Sci. 3 (1), 97–103. https://doi.org/10.1002/jqs.3390030111.

Glasser, N.F., Holt, T.O., Evans, Z.D., Davies, B.J., Pelto, M., Harrison, S., 2016. Recent spatial and temporal variations in debris cover on Patagonian glaciers. Geomorphology 273, 202–216. https://doi.org/10.1016/j.geomorph.2016.07.036.

Gomez, C., Hayakawa, Y., Obanawa, H., 2015. A study of Japanese landscapes using structure from motion derived DSMs and DEMs based on historical aerial photographs: New opportunities for vegetation monitoring and diachronic geomorphology. Geomorphology 242, 11–20. https://doi.org/10.1016/j.geomorph.2015.02.021.

Grindvik-Knudsen, C., Larsen, E., Sejrup, H.P., Stalsberg, K., 2006. Hummocky moraine landscape on Jæren, SW Norway—implications for glacier dynamics during the last deglaciation. Geomorphology 77, 153–168. https://doi.org/10.1016/j.geomorph.2005.12.011.

Häberle, T., 1991. Holocene glacial history of the Hörgádalur area, Tröllaskagi, northern Iceland. En: Maizels JK and Caseldine C (eds) Environmental Change in Iceland: Past and Present. Dordrecht: Kluwer Academic Publishers, 193–202. doi: https://doi.org/10.1007/978-94-011-3150-6_13.

Hambrey, M.J., Quincey, D.J., Glasser, N.F., Reynolds, J.M., Richardson, S.J., Clemmens, S., 2008. Sedimentological, geomorphological and dynamic context of debris-mantled glaciers, Mount Everest (Sagarmatha) region, Nepal. Quat. Sci. Rev. 27, 2361–2389. https://doi.org/10.1016/j.quascirev.2008.08.010.

Hamilton, S.J., Whalley, W.B., 1995a. Preliminary results from the lichenometric study of the Nautardálur rock glacier, Tröllaskagi, northern Iceland. Geomorphology 12, 123–132. https://doi.org/10.1016/0169-555X(94)00083-4.

Hamilton, S.J., Whalley, W.B., 1995b. Rock glacier nomenclature: a re-assessment. Geomorphology 14, 73–80. https://doi.org/10.1016/0169-555X(95)00036-5.

Helama, S., Jones, P.D., Briffa, K.R., 2017. Dark Ages Cold Period: a literature review and directions for future research. The Holocene 27 (10), 1600–1606. https://doi.org/10.1177/0959683617693898.

Herreid, S., Pellicciotti, F., 2020. The state of rock debris covering Earth's glaciers. Nat. Geosci. 13 (9), 621–627. https://doi.org/10.1038/s41561-020-0615-0.

Hippolyte, J.C., Bourlès, D., Braucher, R., Carcaillet, J., Lèanni, L., Arnold, M., Aumaitre, G., 2009. Cosmogenic ^{10}Be dating of a sackung and its faulted rock glaciers, in the Alps of Savoy (France). Geomorphology 108 (3), 312–320. https://doi.org/10.1016/j.geomorph.2009.02.024.

Icelandic Land Survey, d. Consulted from 2017 to 2020 https://www.lmi.is/is.
Innes, J.L., 1985. Lichenometric dating of debris-flow deposits on alpine colluvial fans in southwest Norway. Earth Surf. Process. Landf. 10 (5), 519–524. https://doi.org/10.1002/esp.3290100510.
Ipsen, H.A., Principato, S.M., Grube, R.E., Lee, J.F., 2018. Spatial analysis of cirques from three regions of Iceland: implications for cirque formation and palaeoclimate. Boreas 47, 565–576. https://doi.org/10.1111/bor.12295.
Ivy-Ochs, S., Synal, H.-A., Roth, C., Schaller, M., 2004. Initial results from isotope dilution for Cl and ^{36}Cl measurements at the PSI/ETH Zurich AMS facility. Nucl. Instruments Methods Phys. Res. Sect. B Beam Interact. Mater. Atoms 223–224, 623–627. https://doi.org/10.1016/J.NIMB.2004.04.115.
James, W.H.M., Carrivick, J.L., 2016. Automated modelling of spatially-distributed glacier ice thickness and volume. Comput. Geosci. 92, 90–103. https://doi.org/10.1016/j.cageo.2016.04.007.
Janke, J.R., Regmi, N.R., Giardino, J.R., Vitek, J.D., 2013. Rock glaciers. In: Shroder, J., Giardino, R., Harbor, J. (Eds.), Treatise on Geomorphology. Vol. 8: Glacial and Periglacial Geomorphology. Academic Press, San Diego, CA, pp. 238–273 https://doi.org/10.1016/B978-0-12-374739-6.00211-6.
Janke, J.R., Bellisario, A.C., Ferrando, F.A., 2015. Classification of debris-covered glaciers and rock glaciers in the Andes of central Chile. Geomorphology 241, 98–121. https://doi.org/10.1016/j.geomorph.2015.03.034.
Jomelli, V., Chapron, E., Favier, V., Rinterknecht, V., Braucher, R., Tournier, N., Gascoin, S., Marti, R., Galop, D., Binet, S., Deschamps-Berger, C., Tissoux, H., ASTER Team, 2020. Glacier fluctuations during the Late Glacial and Holocene on the Ariege valley, northern slope of the Pyrenees and reconstructed climatic conditions. Mediterranean. Geosci. Rev. 2, 37–51. https://doi.org/10.1007/s42990-020-00018-5.
Jones, D.B., Harrison, S., Anderson, K., 2019. Mountain glacier-to-rock glacier transition. Glob. Planet. Chang. 181, 102999. https://doi.org/10.1016/j.gloplacha.2019.102999.
Jónsson, Ó.B., 1976. Berghlaup. Ræktunarfélag Norðurlands, Akureyri 623 pp.
Kääb, A., Jacquemart, M., Gilbert, A., Leinss, S., Girod, L., Huggel, C., ... Dokukin, M., 2021. Sudden large-volume detachments of low-angle mountain glaciers–more frequent than thought. Cryosphere Discuss., 151751–151785 https://doi.org/10.5194/tc-2020-243.
Kellerer-Pirklbauer, A., Wangensteen, B., Farbrot, H., Etzelmüller, B., 2007. Relative surface age-dating of rock glacier systems near Hólar in Hjaltadalur, northern Iceland. J. Quat. Sci. 23, 137–151. https://doi.org/10.1002/jqs.1117.
Kellerer-Pirklbauer, A., Lieb, G.K., Avian, M., Gspurning, J., 2008. The response of partially debris-covered valley glaciers to climate change: the example of the Pasterze Glacier (Austria) in the period 1964 to 2006. Geogr. Ann. 90, 269–285. https://doi.org/10.1111/j.1468-0459.2008.00345.x.
Kirkbride, M.P., 2000. Ice-marginal geomorphology and Holocene expansion of debris-covered Tasman glacier, New Zealand. In: Nakawo, M., Raymond, C.F., Fountain, A. (Eds.), Debris-covered Glaciers. 264. IAHS , pp. 211–217. http://hydrologie.org/redbooks/a264/iahs_264_0211.pdf.
Kirkbride, M.P., 2011. Debris-covered glaciers. In: Singh, V.P., Singh, P., Haritashya, U.K. (Eds.), Encyclopedia of Snow, Ice and Glaciers: Encyclopedia of Earth Series. Springer, Netherlands, pp. 180–182 https://doi.org/10.1007/978-90-481-2642-2_622.
Kirkbride, M.P., Dugmore, A.J., 2006. Responses of mountain ice caps in central Iceland to Holocene climate change. Quat. Sci. Rev. 25, 1692–1707. https://doi.org/10.1016/j.quascirev.2005.12.004.
Kirkbride, M.P., Dugmore, A.J., 2008. Two millennia of glacier advances from southern Iceland dated by tephrochronology. Quat. Res. 70, 398–411. https://doi.org/10.1016/j.yqres.2008.07.001.
Knight, J., Harrison, S., 2014. Mountain glacial and paraglacial environments under global climate change: lessons from the past, future directions and policy implications. Geogr. Ann. A Phys. Geogr. 96 (3), 245–264. https://doi.org/10.1111/geoa.12051.
Knight, J., Harrison, S., Jones, D.B., 2019. Rock glaciers and the geomorphological evolution of deglacierizing mountains. Geomorphology 324, 14–24. https://doi.org/10.1016/j.geomorph.2018.09.020.
Kugelmann, O., 1991. Dating recent glacier advances in the Svarfadardalur-Skíðadalur area of Northern Iceland by means of a new lichen curve. En: J.K. Maizels, C. Caseldine (Eds.), Environmental Change in Iceland: Past and Present. Springer Netherlands, Dordrecht, 203–217. doi: https://doi.org/10.1007/978-94-011-3150-6_14.
Lambrecht, A., Mayer, C., Hagg, W., Popovnin, V., Rezepkin, A., Lomidze, N., Svanadze, D., 2011. A comparison of glacier melt on debris-covered glaciers in the northern and southern Caucasus. Cryosphere 5, 525–538. https://doi.org/10.1016/j.gloplacha.2009.05.003.
Larsen, D.J., Miller, G.H., Geirsdóttir, Á., Thordarson, T., 2011. A 3000-year varved record of glacier activity and climate change from the proglacial lake Hvítárvatn, Iceland. Quat. Sci. Rev. 30, 2715–2731. https://doi.org/10.1016/j.quascirev.2011.05.026.
Larsen, D.J., Miller, G.H., Geirsdóttir, Á., Ólafsdóttir, S., 2012. Non-linear Holocene climate evolution in the North Atlantic: a high-resolution, multi-proxy record of glacier activity and environmental change from Hvítárvatn, central Iceland. Quat. Sci. Rev. 39, 14–25. https://doi.org/10.1016/j.quascirev.2012.02.006.
Le Roy, M., Deline, P., Carcaillet, J., Schimmelpfennig, I., Ermini, M., ASTER Team, 2017. 10Be exposure dating of the timing of Neoglacial glacier advances in the Ecrins-Pelvoux massif, southern French Alps. Quat. Sci. Rev. 178, 118–138. https://doi.org/10.1016/j.quascirev.2017.10.010.
Li, Y., 2018. Determining topographic shielding from digital elevation models for cosmogenic nuclide analysis: a GIS model for discrete sample sites. J. Mt. Sci. 15, 939–947. https://doi.org/10.1007/s11629-018-4895-4.
Licciardi, J.M., Kurz, M.D., Curtice, J.M., 2006. Cosmogenic 3He production rates from Holocene lava flows in Iceland. Earth Planet. Sci. Lett. 246, 251–264. https://doi.org/10.1016/J.EPSL.2006.03.016.
Licciardi, J.M., Denoncourt, C.L., Finkel, R.C., 2008. Cosmogenic 36Cl production rates from Ca spallation in Iceland. Earth Planet. Sci. Lett. 267, 365–377. https://doi.org/10.1016/j.epsl.2007.11.036.
Lilleøren, K.S., Etzelmüller, B., Gärtner-Roer, I., Kääb, A., Westermann, S., Gumundsson, Á., 2013. The distribution, thermal characteristics and dynamics of permafrost in Tröllaskagi, Northern Iceland, as inferred from the distribution of rock glaciers and ice-cored moraines. Permafr. Periglac. Process. 24 (4), 322–335. https://doi.org/10.1002/ppp.1792.
Linge, H., Nesje, A., Matthews, J.A., Fabel, D., Xu, S., 2020. Evidence for rapid paraglacial formation of rock glaciers in southern Norway from 10Be surface-exposure dating. Quat. Res., 1–16 https://doi.org/10.1017/qua.2020.10.
Mackay, S.L., Marchant, D.R., 2016. Dating buried glacier ice using cosmogenic 3He in surface clasts: Theory and application to Mullins Glacier, Antarctica. Quat. Sci. Rev. 140, 75–100. https://doi.org/10.1016/j.quascirev.2016.03.013.
Maizels, J.K., Dugmore, A.J., 1985. Lichenometric dating and tephrochronology of sandur deposits, Sólheimajökull area, southern Iceland. Jökull 35, 69–78.
Marrero, S.M., Phillips, F.M., Caffee, M.W., Gosse, J.C., 2016. CRONUS-Earth cosmogenic 36Cl calibration. Quat. Geochronol. 31, 199–219. https://doi.org/10.1016/j.quageo.2015.10.002.
Martin, H.E., Whalley, B., Orr, J., Caseldine, C., 1994. Dating and interpretation of rock glaciers using lichenometry, south Tröllaskagi, North Iceland. In: Stötter, J., Wilhelm, F. (Eds.), Environmental change in Iceland, Münchener Geographische Abhandlungen, Reihe B. 12, pp. 205–224.
Mayr, E., Hagg, W., 2019. Debris-covered glaciers. In: Heckmann, T., Morche, D. (Eds.), Geomorphology of Proglacial Systems, Geography of the Physical Environment, pp. 59–71 https://doi.org/10.1007/978-3-319-94184-4_4.
Meier, M.F., Post, A.S., 1962. Recent variations in mass net budgets of glaciers in western North America. Int. Assoc. Hydrol. Sci. Publ. 58, 63–77.
Merchel, S., Bremser, W., Alfimov, V., Arnold, M., Aumaître, G., Benedetti, L., Bourlès, D.L., Caffee, M., Fifield, L.K., Finkel, R.C., Freeman, S.P.H.T., Martschini, M., Matsushi, Y., Rood, D.H., Sasa, K., Steier, P., Takahashi, T., Tamari, M., Tims, S.G., Tosaki, Y., Wilcken, K.M., Xu, S., 2011. Ultra-trace analysis of 36Cl by accelerator mass spectrometry: an interlaboratory study. Anal. Bioanal. Chem. 400, 3125–3132. https://doi.org/10.1007/s00216-011-4979-2.
Mercier, D., Cossart, E., Decaulne, A., Feuillet, T., Jónsson, H.P., Sæmundsson, Þ., 2013. The Höfðahólar rock avalanche (sturzström): chronological constraint of paraglacial landsliding on an Icelandic hillslope. The Holocene 23, 432–446. https://doi.org/10.1177/0959683612463104.
Micheletti, N., Chandler, J.H., Lane, S.N., 2014. Investigating the geomorphological potential of freely available and accessible structure from motion photogrammetry using a smartphone. Earth Surf. Process. Landf. https://doi.org/10.1002/esp.3648.
Micheletti, N., Chandler, J.H., Lane, S.N., 2015. Structure From Motion (SfM) Photogrammetry. British Society for Geomorphology. Geomorphological Techniques, Cap. 2, Sec. 2.2.
Miller, G.H., Brigham-Grette, J., Alley, R.B., Anderson, L., Bauch, H.A., Douglas, M.S.V., Edwards, M.E., Elias, S.A., Finney, B.P., Fitzpatrick, J.J., Funder, S.V., Herbert, T.D., Hinzman, L.D., Kaufman, D.S., MacDonald, G.M., Polyak, L., Robock, A., Serreze, M.C., Smol, J.P., Spielhagen, R., White, J.W.C., Wolfe, A.P., Wolff, E.W., 2010. Temperature and precipitation history of the Arctic. Quat. Sci. Rev. 29, 1679–1715. https://doi.org/10.1016/j.quascirev.2010.03.001.
Monnier, S., Kinnard, C., 2015. Reconsidering the glacier to rock glacier transformation problem: New insights from the central Andes of Chile. Geomorphology 238, 47–55. https://doi.org/10.1016/j.geomorph.2015.02.025.
Monnier, S., Kinnard, C., 2016. Pluri-decadal (1955–2014) evolution of glacier–rock glacier transitional landforms in the central Andes of Chile (30–33° S). Earth Surf. Dyn. 5, 493–509. https://doi.org/10.5194/esurf-5-493-2017.
Monnier, S., Kinnard, C., Surazakov, A., Bossy, W., 2014. Geomorphology, internal sctructure, and successive development of a glacier foreland in the semiarid Chilean Andes (Cerro Tapado, upper Elqui Valley, 30° 08′ S., 69° 55′ W). Geomorphology 207, 126–140. https://doi.org/10.1016/j.geomorph.2013.10.031.
Moran, A.P., Ivy-Ochs, S., Vockenhuber, C., Kerschner, H., 2016. Rock glacier development in the northern calcareous Alps at the pleistocene-Holocene boundary. Geomorphology 273, 178–188. https://doi.org/10.1016/j.geomorph.2016.08.017.
Morino, C., Conway, S.J., Sæmundsson, Þ., Kristinsson, J.H., Hillier, Butcher, F., Balme, M.R., Colm, J., Argles, T., 2019. Molards as a marker of permafrost degradation and landslide processes. Earth Planet. Sci. Lett. 516, 136–147. https://doi.org/10.1016/j.epsl.2019.03.040.
Norðdahl, H., Pétursson, H.G., 2005. Relative sea level changes in Iceland. New aspects of the Weichselian deglaciation of Iceland. In: Caseldine, C., Russel, A., Harðardóttir, J., Knudsen, Ó. (Eds.), Iceland - Modern Processes and Past Environments, 25–78. Elsevier, Amsterdam.
Norðdahl, H., Ingólfsson, Ó., Pétursson, H.G., Hallsdóttir, M., 2008. Late Weichselian and Holocene environmental history of Iceland. Jökull 58, 343–364.
Ogilvie, A.E., Jónsson, T., 2001. "Little Ice Age" research: a perspective from Iceland. Clim. Chang. 48 (1), 9–52. https://doi.org/10.1023/A:1005625729889.
Osmaston, H., 2005. Estimates of glacier equilibrium line altitudes by the Area × Altitude, the Area × Altitude Balance Ratio and the Area × Altitude Balance Index methods and their validation. Quat. Int. 138–139, 22–31. https://doi.org/10.1016/j.quaint.2005.02.004.
Palacios, D., Ortiz, Gómez, Andrés, N., Salvador, F., Oliva, M., 2016. A timing and new geomorphologic evidence of the last deglaciation stages in Sierra Nevada (southern Spain). Quat. Sci. Rev. 150, 110–129. https://doi.org/10.1016/j.quascirev.2016.08.012.
Palacios, D., Andrés, N., García-Ruiz, J.M., Schimmelpfennig, I., Campos, N., Léanni, L., Team, Aster, 2017. Deglaciation in the central Pyrenees during the Pleistocene–Holocene transition: timing and geomorphological significance. Quat. Sci. Rev. 150, 110–129. https://doi.org/10.1016/j.quascirev.2017.03.007.
Palacios, D., Oliva, M., Gómez-Ortiz, A., Andrés, N., Fernández-Fernández, J.M., Schimmelpfennig, I., ... Team, A.S.T.E.R., 2020. Climate sensitivity and geomorphological response of cirque glaciers from the late glacial to the Holocene, Sierra Nevada, Spain. Quat. Sci. Rev. 248, 106617. https://doi.org/10.1016/j.quascirev.2020.106617.

Pellitero, R., Rea, B.R., Spagnolo, M., Bakke, J., Hughes, P., Ivy-Ochs, S., Lukas, S., Ribolini, A., 2015. A GIS tool for automatic calculation of glacier equilibrium-line altitudes. Comput. Geosci. 82, 55–62. https://doi.org/10.1016/j.cageo.2015.05.005.

Pellitero, R., Rea, B.R., Spagnolo, M., Bakke, J., Ivy-Ochs, S., Frew, C.R., Hughes, P., Ribolini, A., Lukas, S., Renssen, H., 2016. GlaRe, a GIS tool to reconstruct the 3D surface of palaeoglaciers. Comput. Geosci. 94, 77–85. https://doi.org/10.1016/j.cageo.2016.06.008.

Pétursson, H.G., Norðdahl, H., Ingólfsson, O., 2015. Late Weischelian history of relative sea level changes in Iceland during a collapse and subsequent retreat of marine based ice sheet. Cuad. Invest. Geogr. 41, 261–277. https://doi.org/10.18172/cig.2741.

Porter, S.C., 1975. Equilibrium-line altitudes of late Quaternary glaciers in the Southern Alps, New Zealand. Quat. Res. 5 (1), 27–47. https://doi.org/10.1016/0033-5894(75)90047-2.

Potter, N.J., Steig, E.J., Clark, D.H., Speece, M.A., Clark, G.M., Updike, A.B., 1998. Galena Creek rock glacier revisited—new observations on an old controversy. Geogr. Ann. Ser. A. Phys. Geogr. 80, 251–265. https://doi.org/10.1111/j.0435-3676.1998.00041.x.

Quincey, D.J., Glasser, N.F., 2009. Morphological and ice-dynamical changes on the Tasman Glacier, New Zealand, 1990–2007. Glob. Planet. Chang. 68, 185–197. https://doi.org/10.1016/j.gloplacha.2009.05.003.

Rodríguez-Mena, M., Fernández-Fernández, J.M., Tanarro, L.M., Zamorano, J.J., Palacios, D., 2021. Héðinsdalsjökull, northern Iceland: geomorphology recording the recent complex evolution of a glacier. J. Maps 17 (2), 301–313. https://doi.org/10.1080/17445647.2021.1920056.

Rowan, A.V., Egholm, D.L., Quincey, D.J., Glasser, N.F., 2015. Modelling the feedbacks between mass balance, ice flow and debris transport to predict the response to climate change of debris-covered glaciers in the Himalaya. Earth Planet. Sci. Lett. 430, 427–438. https://doi.org/10.1016/j.epsl.2015.09.004.

Sæmundsson, K., Kristjansson, L., McDougall, I., Watkins, N.D., 1980. K-Ar dating, geological and paleomagnetic study of a 5-km lava succession in northern Iceland. J. Geophys. Res. Solid Earth 85, 3628–3646. https://doi.org/10.1029/JB085iB07p03628.

Sæmundsson, Þ., Morino, C., Helgason, J.K., Conway, S.J., Pétursson, H.G., 2018. The triggering factors of the Móafellshyrna debris slide in northern Iceland: intense precipitation, earthquake activity and thawing of mountain permafrost. Sci. Total Environ. 621, 1163–1175. https://doi.org/10.1016/J.SCITOTENV.2017.10.111.

Scherler, D., Egholm, D.L., 2020. Production and transport of supraglacial debris: insights from cosmogenic 10Be and numerical modeling, Chhota Shigri Glacier, Indian Himalaya. J. Geophys. Res. Earth Surf. 125 (10), e2020JF005586. https://doi.org/10.1029/2020JF005586.

Schimmelpfennig, I., Benedetti, L., Finkel, R., Pik, R., Blard, P.H., Bourlès, D., Burnard, P., Williams, A., 2009. Sources of in-situ ^{36}Cl in basaltic rocks. Implications for calibration of production rates. Quat. Geochronol. 4, 441–461. https://doi.org/10.1016/j.quageo.2009.06.003.

Schimmelpfennig, I., Benedetti, L., Garreta, V., Pik, R., Blard, P.H., Burnard, P., Bourlès, D., Finkel, R., Ammon, K., Dunai, T., 2011. Calibration of cosmogenic 36Cl production rates from Ca and K spallation in lava flows from Mt. Etna (38°N, Italy) and Payun Matru (36°S, Argentina). Geochim. Cosmochim. Acta 75, 2611–2632. https://doi.org/10.1016/j.gca.2011.02.013.

Schimmelpfennig, I., Schaefer, J.M., Putnam, A.E., Koffman, T., Benedetti, L., Ivy-Ochs, S., Schlüchter, C., Arnold, M., Aumaître, G., Bourlès, D., Keddadouche, K., 2014. ^{36}Cl production rate from K-spallation in the European Alps (Chironico landslide, Switzerland). J. Quat. Sci. 29, 407–413. https://doi.org/10.1002/jqs.2720.

Shukla, A., Gupta, R.P., Arora, M.K., 2009. Estimation of debris cover and its temporal variation using optical satellite sensor data: a case study in Chenab basin, Himalaya. J. Glaciol. 55 (191), 444–452. https://doi.org/10.3189/002214309788816632.

Spreafico, M.C., Sternai, P., Agliardi, F., 2021. Paraglacial rock-slope deformations: sudden or delayed response? Insights from an integrated numerical modelling approach. Landslides 18, 1311–1326. https://doi.org/10.1007/s10346-020-01560-x.

Steinemann, O., Reitner, J.M., Ivy-Ochs, S., Christl, M., Synal, H.A., 2020. Tracking rockglacier evolution in the Eastern Alps from the Lateglacial to the early Holocene. Quat. Sci. Rev. 241, 106424. https://doi.org/10.1016/j.quascirev.2020.106424.

Stone, J.O., 2000. Air pressure and cosmogenic isotope production. J. Geophys. Res. Solid Earth 105, 23753–23759. https://doi.org/10.1029/2000JB900181.

Stone, J.O., Allan, G.L., Fifield, L.K., Cresswell, R.G., 1996. Cosmogenic chlorine-36 from calcium spallation. Geochim. Cosmochim. Acta 60, 679–692. https://doi.org/10.1016/0016-7037(95)00429-7.

Stone, J.O., Fifielde, K., Vasconcelos, P., 2005. Terrestrial chlorine-36 production from spallation of iron. Abstract of 10th International Conference on Accelerator Mass Spectrometry. CA, Berkeley.

Storni, E., Hugentobler, M., Manconi, A., Loew, S., 2020. Monitoring and analysis of active rockslide-glacier interactions (Moosfluh, Switzerland). Geomorphology 371, 107414. https://doi.org/10.1016/j.geomorph.2020.107414.

Stötter, J., 1990. Geomorphologische und landschaftsgeschichtliche Untersuchungen im Svarfaðardalur-Skíðadalur, Tröllaskagi, N-Island. Münchener Geogr. Reihe B, Abhandlungen.

Stötter, J., Wastl, M., Caseldine, C., Häberle, T., 1999. Holocene palaeoclimatic reconstruction in northern Iceland: Approaches and results. Quat. Sci. Rev. 18, 457–474. https://doi.org/10.1016/S0277-3791(98)00029-8.

Striberger, J., Björck, S., Benediktsson, Í.Ö., Snowball, I., Uvo, C.B., Ingólfsson, Ó., Kjær, K.H., 2011. Climatic control of the surge periodicity of an Icelandic outlet glacier. J. Quat. Sci. 26 (6), 561–565. https://doi.org/10.1002/jqs.1527.

Striberger, J., Björck, S., Holmgren, S., Hamerlík, L., 2012. The sediments of Lake Lögurinn–a unique proxy record of Holocene glacial meltwater variability in eastern Iceland. Quat. Sci. Rev. 38, 76–88. https://doi.org/10.1016/j.quascirev.2012.02.001.

Tanarro, L.M., Palacios, D., Zamorano, J.J., Andrés, N., 2018. Proposal for geomorphological mapping of debris-covered and rock-glaciers and its application to Tröllaskagi Peninsula (Nothern Iceland). J. Maps 14 (2), 692–703. https://doi.org/10.1080/17445647.2018.1539417.

Tanarro, L.M., Palacios, D., Andrés, N., Fernández-Fernández, J.M., Zamorano, J.J., Sæmundsson, Þ., Brynjólfsson, S., 2019. Unchanged surface morphology in debris-covered glaciers and rock glaciers in Tröllaskagi peninsula (northern Iceland). Sci. Total Environ. 648, 218–235. https://doi.org/10.1016/j.scitotenv.2018.07.460.

Thakuri, S., Salerno, F., Smiraglia, C., Bolch, T., D'Agata, C., Viviano, G., Tartari, G., 2014. Tracing Glacier Changes Since the 1960s on the South Slope of Mt. Everest (Central Southern Himalaya) Using Optical Satellite Imagery. https://doi.org/10.5194/tc-8-1297-2014.

Thompson, A., Jones, A., 1986. Rates and causes of proglacial river terrace formation in southeast Iceland: an application of lichenometric dating techniques. Boreas 15 (3), 231–246. https://doi.org/10.1111/j.1502-3885.1986.tb00928.x.

Tielidze, L.G., Bolch, T., Wheate, R.D., Kutuzov, S.S., Lavrentiev, I.I., Zemp, M., 2020. Supraglacial debris cover changes in the Greater Caucasus from 1986 to 2014. Cryosphere 14, 585–598. https://doi.org/10.5194/tc-14-585-2020.

Uppala, S.M., Kållberg, P.W., Simmons, A.J., Andrae, U., da Costa Bechtold, V., Fiorino, M., Gibson, J.K., Haseler, J., Hernandez, A., Kelly, G.A., Li, X., Onogi, K., Saarinen, S., Sokka, N., Allan, R.P., Andersson, E., Arpe, K., Balmaseda, M.A., Beljaars, A.C.M., van de Berg, L., Bidlot, J., Bormann, N., Caires, S., Chevallier, F., Dethof, A., Dragosavac, M., Fisher, M., Fuentes, M., Hagemann, S., Hólm, E., Hoskins, B.J., Isaksen, L., Janssen, P.A.E.M., Jenne, R., McNally, A.P., Mahfouf, J.F., Morcrette, J.J., Rayner, N.A., Saunders, R.W., Simon, P., Sterl, A., Trenberth, K.E., Untch, A., Vasiljevic, D., Viterbo, P., Woollen, J., 2005. The ERA-40 re-analysis. Q. J. R. Meteorol. Soc. 131, 2961–3012. https://doi.org/10.1256/qj.04.176.

Vacco, D.A., Alley, R.B., Pollard, D., 2010. Glacial advance and stagnation caused by rock avalanches. Earth Planet. Sci. Lett. 294 (1–2), 123–130. https://doi.org/10.1016/j.epsl.2010.03.019.

Van der Veen, C.J., 1999. Fundamentals of Glacier Dynamics. Balkema, Rotterdam 462 pp.

Wangensteen, B., Gudmundsson, A., Eiken, T., Kääb, A., Farbrot, H., Etzelmüller, B., 2006. Surface displacements and surface age estimates for creeping slope landforms in Northern and Eastern Iceland using digital photogrammetry. Geomorphology 80, 59–79. https://doi.org/10.1016/j.geomorph.2006.01.034.

Whalley, W.B., Martin, H.E., 1992. Rock glaciers: II models and mechanisms. Prog. Phys. Geogr. 16 (2), 127–186. https://doi.org/10.1177/030913339201600201.

Whalley, W.B., Douglas, G.R., Jonsson, A., 1983. The magnitude and frequency of large rockslides in Iceland in the postglacial. Geogr. Ann. A Phys. Geogr. 65, 99–110. https://doi.org/10.2307/520724.

Whalley, W.B., Hamilton, S., Palmer, C., Gordon, J., Martin, H.E., 1995. The dynamics of rock glaciers: data from Tröllaskagi, North Iceland. In: Slaymaker, O. (Ed.), Steepland Geomorphology. John Wiley & Sons, pp. 129–145.

Winkler, S., Lambiel, C., 2018. Age constraints of rock glaciers in the Southern Alps/New Zealand–Exploring their palaeoclimatic potential. The Holocene 28 (5), 778–790. https://doi.org/10.1177/0959683618756802.